



FEDERAL UNIVERSITY OF ESPÍRITO SANTO
DEPARTMENT OF ENVIRONMENTAL ENGINEERING
ENVIRONMENTAL ENGINEERING GRADUATE PROGRAM

BY

THAÍS NUNES COUTINHO

**A MEDIUM-TERM SEABED MORPHOLOGICAL EVOLUTION IN THE BARRA
DO RIACHO'S PORT AND ITS SURROUNDINGS, ES-BRASIL.**

VITÓRIA
2019

THAÍS NUNES COUTINHO

**MEDIUM-TERM SEABED MORPHOLOGICAL EVOLUTION IN THE BARRA DO
RIACHO'S PORT AND ITS SURROUNDINGS, ES-BRASIL**

Dissertation submitted in partial fulfillment of the requirements for the degree of Master of Environmental Engineering in the Environmental Engineering Graduate Program, Federal University of Espírito Santo.

Advisor: Prof. Dr. Julio Tomás Aquije Chacaltana

VITÓRIA
2019

AGRADECIMENTOS

São tantas as pessoas que contribuíram tanto tecnicamente quanto emocionalmente neste trabalho que gostaria de pedir desculpas se esqueci de alguém, por isso já deixo aqui registrado meus sinceros agradecimentos a todos os envolvidos.

A Deus por me incentivar em espírito a sempre persistir mesmo nas dificuldades que encontrei que me fizeram pensar em desistir. A Ti lhe dedico este trabalho.

Ao meu querido, Leonardo, companheiro de todas as horas que me apoiou em não desistir nunca dos meus sonhos que se tornaram nossos.

A minha família, Bete, Venicius, Lorena e Nicole pelo carinho, risadas, companheirismo e por compreender minha ausência para elaboração deste trabalho.

Ao meu orientador, Dr. Julio Tomás Aquije Chacaltana, pela confiança em meu trabalho, por acreditar em mim, pelo apoio, sugestões e incentivo que levarei para vida.

A professora Dra. Jacqueline Albino, pela confiança, sugestões, ideias e apoio neste trabalho.

Ao professor Dr. Diogo Buarque pela confiança em mim, apoio na parte burocrática da dissertação e ideias e sugestões que contribuíram para este trabalho.

A Prussia Piumbini e ao Thiago Nascimento, em nome da UMISAN, pelo auxílio na solicitação dos dados e a Portocel pela concessão dos dados para elaboração deste trabalho.

Ao Fernando Corleto e ao Claudio Dalle Olle, em nome do IEMA, pela concessão dos estudos ambientais da região que auxiliaram na elaboração da dissertação.

À Jade Boscaglia pelo tempo e carinho que tirou para contribuir com ideias na dissertação.

Aos amigos, Fábio, Kelly, Fran e Kaio do Labesul, por todo o apoio, carinho e ideias durante a escrita da dissertação e momentos de alegria que passamos.

Aos amigos que entenderam minha ausência, Noemia, André, Hugo, Hamilton e Vitor Leonardo, pelo apoio, carinho e risadas nos momentos de desespero.

A Gabi, em nome da Control Ambiental, pelo apoio, carinho e confiança em mim depositada que me permitiu trabalhar ao mesmo tempo do desenvolvimento deste trabalho. Muito obrigada.

ABSTRACT

Due to the necessity to predict the morphological changes in shoreline, bar migration, estuary dynamic and in ports logistics the sediment transport and morphology bed changes appear as an important theme, mainly. In this work the seabed changes induced by tide, waves and wind in port of Portocel surroundings located at Barra do Riacho, Brazil was studied. The hydrodynamic induced by wave-current interaction was obtained by coupling of shallow water equation with the spectral wave model based on the wave spectral action balance equation. These coupled models are connected through the radiation stress and are solved numerically. The morphological seabed changes are expressed by the seabed sediment mass conservation equation in which four morphological acceleration factors (1, 30, 60 and 90) were tested. It was found a good agreement between model results and measured currents, water levels, significant wave height, peak period, mean direction and net seabed morphology changes. The results of both bedload and suspended sediment transport rates showed that the highest sediment transport rates are located at the north and south of the port. These results are associated with morphological changes in surroundings of the coast. Morphological seabed changes for 20 years considering waves, wind and tide conditions using morphological acceleration factor equal to 90 shown erosion and depositions rates from 2 m (erosion) to 2.33 m (deposition) in north of port, which was the highest erosion and deposition areas. Results suggest that the waves and tidal elevations are the main physical processes that drive seabed morphology changes leading to erosion near the coast driven by wave breaking and its resulting currents, which transport sediments.

Keywords: numerical modelling, sediment transport, morphological seabed changes

RESUMO

O transporte de sedimento e as mudanças morfológicas do leito tem sido um tema de grande relevância, principalmente, devido a necessidade de prever as mudanças morfológicas na linha de costa, migração de barras, dinâmica estuarina e logística de portos. Neste trabalho, as mudanças do leito induzidas por maré, onda e vento no porto de Portocel e proximidades, localizados em Barra do Riacho, foram estudados. A hidrodinâmica induzida por correntes geradas por ondas foi obtida pelo acoplamento da equação de águas rasas com um modelo de ondas espectral baseado na equação do balanço de densidade da ação espectral. Estes modelos acoplados são conectados através das tensões de radiação da onda e são resolvidos numericamente. As mudanças morfológicas do leito são expressas pela equação de conservação da massa de sedimento de fundo em que quatro fatores de aceleração da morfologia foram testados (1, 30, 60 e 90). Os resultados encontrados mostram bons ajustes entre o modelo numérico e os dados medidos de correntes, nível d'água, altura significativa, período de pico, direção média e mudanças morfológicas do leito. As taxas de transporte de sedimento residuais de fundo e em suspensão mostram que as maiores taxas de transporte de sedimento estão localizadas ao norte e ao sul do porto. Estes resultados estão associados com as mudanças morfológicas nas proximidades da costa. As mudanças morfológicas para 20 anos, considerando ondas, vento e maré com o uso do fator de aceleração da morfologia igual a 90 mostraram taxas de erosão e deposição de 2 m (erosão) a 2,33 m (deposição) ao norte do porto, em que foram as regiões com as maiores taxas de erosão e deposição. Os resultados sugerem que ondas e marés são os principais processos que governam as mudanças morfológicas do leito, levando a erosão próximo à costa, dirigida pelas ondas que quebram e resultam em correntes que transportam sedimentos.

Palavras-chave: modelagem numérica, transporte de sedimento, mudanças morfológicas do leito.

LIST OF FIGURES

Figure 4-1 – Map showing the Barra do Riacho’s Port and Jurong shipyard located in Aracruz, Brazil.	22
Figure 4-2 – Numerical grid used to represent hydro-morphological processes in Barra do Riacho’s port, located at Barra do Riacho, Aracruz. In (a) the full grid and (b) a zoom at the Barra do Riacho’s port.	26
Figure 4-3 – Bathymetry provided by in situ measures and nautical charts digitalized for numerical grid.	27
Figure 4-4 – Sedimentological distribution interpolated for computational domain.	28
Figure 4-5 – Flowchart showing the coupling between the hydrodynamic and wave models.	32
Figure 4-6 – Flowchart showing the interaction between wave, hydrodynamic, sediment transport and morphological evolution models.	36
Figure 5-1 - Comparison of significant wave height, wave direction and wave peak period observed (dots) and modelled (solid line) during May 17 and June 16 of 2009.	40
Figure 5-2 - Comparison of velocities considering tide (green line), tide and wind (magenta line) and tide, wind and wave (blue line) with observed data (black dots) in (a). Same for water levels in (b).	42
Figure 5-3 – Morphological net changes in situ (a) and modelled (b) in port of Portocel for 1 year (2010 – 2011).	44
Figure 5-4 – Histogram of direction (a), peak period (c) and wave height (e) and energy spectrum of directions x wave height (b), peak period x direction (d) and wave height x peak period (f) in port of Portocel. Data source: SMC-DOW.	46
Figure 5-5 – Significant wave height (m) distribution and mean direction of wave propagation using 60 years SMC climatology data as boundary conditions.	48
Figure 5-6 - Velocities in ebb and flood tidal currents. The figures a and b represent tidal levels in ebb and flood, respectively. The figures c, e and g represent tide only, tide and wind and tide, wind and wave, respectively in ebb cycle and the figures d, and h are tide only, tide and wind and tide, wind and wave, respectively in flood cycle.	50
Figure 5-7: Net suspended sediment transport rate in Port of Portocel and surroundings.	52
Figure 5-8 – Net bedload sediment transport rate in the Port of Portocel and surroundings.	53
Figure 5-9 – Predicted bathymetries under different Morfac value 1 (a), 30 (b), 60 (c) and 90 (d).	54
Figure 5-10 – Morphological evolution in port of Portocel using Morfac = 90 for 1 year (a), 2.5 years (b), 5 years (c), 10 years (d), 15 years (e) and 20 years (f). Blue is erosion patterns and red is the deposition patterns.	56
Figure 5-11 – Morphological profiles P1 (a), P2 (b) and P3 (c) located in north, south and inside the port of Portocel for initial profile (black line), 1 year (green line), 2.5 years (magenta line), 5 years (dark green line), 10 years (mustard line), 15 years (purple line) and 20 years (blue line).	59

LIST OF TABLES

Table 4-1 – Bathymetry historical data.	25
Table 4-2 – Statistics parameters and their meaning utilized in numerical model validation.....	37
Table 5-1 – Statistical parameters in terms of significant wave height (H_s), wave direction and wave peak period (T_p).....	41
Table 5-2 – Statistics parameters for measured and modelled velocities and water levels.	43
Table 5-3 – Statistics wave parameters in study region from 1948 to 2008 from DOW database.....	45

SYMBOLS

\vec{c}_g – group wave velocity [m. s⁻¹]

D_* - dimensionless grain size [-]

E_{ev} – evaporation rate per unit area [$m\ s^{-1}$]

F_u, F_v – horizontal Reynold's stresses by area unit in x and y directions [$kg\ m^{-1}\ s^{-2}$]

M_e – erosion parameter [$kg.m^{-2}\ s^{-1}$]

P_o – reference pressure [N.m²]

P_z – total pressure at z -level [N.m²]

\vec{U} – depth-averaged horizontal velocity vector [m.s⁻¹]

U_{cr} – critical velocity [m/s]

U_e – effective velocity [m/s]

c_σ, c_θ – spectral velocities [m. s⁻¹]

d_{50} – median diameter of sediment [m]

$f_{morphofac}$ – morphological acceleration factor [-]

q_b – bed-load sediment transport per unit of time [$m^2\ s^{-1}$]

q_{in} – local source per unit volume [s^{-1}]

q_{out} – local sink per unit volume [s^{-1}]

q_s – suspended sediment transport rate [$m^{-3}s^{-1}.m^{-1}$]

w_s – settling velocity [$m\ s^{-1}$]

z_b – seabed elevation [m]

ν_v – vertical eddy viscosity [$m^2\ s^{-1}$]

ρ_0 – reference density of water [$kg\ m^{-3}$]

σ_f – relative wave frequency [s^{-1}]

τ_{bx}, τ_{by} – bed shear stress in x and y directions [$kg\ m^{-1}\ s^{-2}$]

τ_{ce}, τ_{cd} – user specified critical erosion and deposition shear stresses [$kg\ m^{-1}\ s^{-2}$]

h – still water depth [m]

$\Delta t_{hidrodinâmico}$ – hydrodynamic time step [s]
 Δt_{morf} – morphological time step [s]
 D – deposition rate [$m s^{-1}$]
 E – erosion rate [$m s^{-1}$]
 H – total water depth [m]
 N – energy density of wave [$J.s.m^{-2}$]
 P – hydrostatic water pressure [$kg m^{-1} s^{-2}$]
 P – precipitation [$m s^{-1}$]
 Q – global source or sink per unit area [$m s^{-1}$]
 S – source and sink term [$J.m^{-2}.s$]
 U – magnitude of depth –averaged horizontal velocity [$m.s^{-1}$]
 c – suspended sediment concentration [$kg m^{-3}$]
 d – still water depth [m]
 f – Coriolis parameter [s^{-1}]
 g – acceleration due to gravity [$m s^{-2}$]
 s – relative density of sediment fraction. [-]
 t – time [s]
 u, v, w – flow velocities in x, y, z directions [$m s^{-1}$]
 x, y, z – co-ordinate system [m]
 ε – porosity [-]
 η – free surface elevation [m]
 θ – direction [rad]
 ρ – density of fluid [$kg m^{-3}$]
 σ – scaled vertical co-ordinate [-]
 σ – scaled vertical co-ordinate system [-]
 τ – bed shear stress [$kg m^{-1} s^{-2}$]
 ω – velocity in z -direction in the σ -co-ordinate system [$m s^{-1}$]

SUMMARY

1	INTRODUCTION	12
2	OBJECTIVES	15
2.1	SPECIFIC OBJECTIVES.....	15
3	LITERATURE REVIEW	16
3.1	MORPHOLOGICAL MODELLING.....	16
3.2	SEABED EVOLUTION IN PORTS AND HARBOURS.....	19
4	METODOLOGY	22
4.1	STUDY AREA.....	22
4.2	HYDRODYNAMICS.....	22
4.2.1	Physical-mathematical model	23
4.2.2	Model set up	25
4.3	WAVES.....	29
4.3.1	Physical-mathematical model	29
4.3.2	Model set up	30
4.4	WAVE-CURRENT COUPLING.....	31
4.5	WIND.....	32
4.6	SEDIMENT TRANSPORT AND SEABED EVOLUTION.....	33
4.7	MODEL VALIDATION AND SCENARIOS.....	37
4.7.1	Model validation	37
4.7.2	Scenarios	38
5	RESULTS AND DISCUSSION	39
5.1	MODELS VALIDATION.....	39
5.1.1	Wave modelling	39
5.1.2	Hydrodynamic modelling	41
5.1.3	Morphological modelling	43
5.2	THE WAVE CLIMATOLOGY.....	44
5.3	THE HYDRODYNAMICS.....	49
5.4	SEDIMENT TRANSPORT.....	51
5.5	MORPHOLOGICAL EVOLUTION.....	53
6	CONCLUSIONS AND RECOMMENDATIONS	60
6.1	CONCLUSIONS.....	60
6.2	RECOMMENDATIONS.....	61

7	REFERENCES.....	62
---	-----------------	----

1 INTRODUCTION

The morphological changes in estuaries and coastal areas has a significant importance because its capacity to absorb wave energy, moderate the water quality, provide relief for tidal surges and recreational uses (DUNN et. al. 2015). Furthermore it has an economic impact, for example, for worldwide logistics with ports and harbors.

Ports and harbors provide many maritime services that include transportation of passengers and goods, and it is relevant to world logistic to import final prices and export competitiveness (DWARAKISH and SALIM, 2015). The presence of a port or harbor in coastal areas includes obstacles that alter the flow and the hydrodynamics. Consequently, the sediment transport dynamics, for example, breakwaters, jetties and quays are barriers that can cause undesired sedimentation of navigation channel and around ports or harbors which requires periodic maintenance dredging (PRUMM and IGLESIAS, 2016).

Dredging is the term given to removing sediments that have been transported by currents and waves to the waterways. In ports and harbors dredging is used to keep navigation channels at defined depths, and it can cost millions of dollars annually. Dredging operations is indispensable to port's management owing to ensure the deepened navigation channel to larger ships that are used in global industry. Moreover, the maintenance of dredging assures the passage of commercial ships and decreases the risks of incidents that could occur in shallower channels, which includes oil spills and groundings (PORTS AUSTRALIA, 2014).

The morphological changes in coastal areas and port management are subjects recently discussed in order to understand the morphological effects and its prediction, which in turn is hard to predict. Kim and Park (2015) utilized statistical models to make predictions of coastal environments with data measured in situ, however, the analyses with numerical models have been shown to be a very efficient tool to study the morphological evolution and processes in coastal areas (LESSER, 2004, 2009; CAYOCCA, 2001; ABANADES et. al., 2014c; WU et. al., 2011, LI, 2010; DUNN et. al., 2015; MAYERLE, et. al., 2015; DISSANAYAKE et. al., 2012).

Despite the difficulty to predict the morphological changes, scientists and engineers are using technological improvements in numerical models for long-term

investigations with calibrated and validated historical data analysis (PRUMM and IGLESIAS, 2016; DISSANAYAKE et. al., 2009; van der WEGEN, 2010).

The understanding of the sediment transport allows comprehending the morphodynamics changes and its effects on operational activities in ports and harbors. Therefore, prediction of morphological changes may allow a more efficient coastal management, reducing dredging operations and the undesirable morphological effects within the estuary and coastal areas.

Moreover, coastal systems are subject to the action of waves and currents which can lead to shoreline changes and seabed morphological changes, for example, sandbar migration, beach erosion and others. Several studies have been conducted to comprehend and analyze these systems, how they are and how they are going to behave in a large or medium time-scale, such as tidal inlets (WANG et. al., 1995, DISSANAYAKE et. al., 2012, WANG et. al., 1995, CAYOCCA, 2001); sandbar migration and beach evolution (RUGGIERO et. al., 2009); beach profile migration; tidal basins (DASTGHEIB et. al. 2008), estuarine systems (van der WEGEN, et. al., 2008), and an interesting approach to analyze the erosion and deposition areas, for example in tidal flats (KUANG et. al., 2013).

Over the years, modelers used 1D models to simulate the morphological changes, however nowadays, 2D depth-averaged models and 3D model are applied to the flow field and sediment motion (SPEARMAN, et. al., 1998; LESSER, 2004). Those models are more often used to obtain long-term responses adopting high spatial and temporal resolutions which provide more detailed description of study area. While the 3D model is applied to obtain depthwise variations of velocity, temperature, salinity and sediment concentration.

Among the numerical models, the Delft3D model is a state-of-the-art model to simulate sediment transport and hydrodynamics. This model has been applied to study the morphological bed evolution in estuarine and coastal regions (DISSANAYAKE et. al., 2009; DISSANAYAKE et. al., 2012; DASTGHEIB et. al. 2008, PRUMM and IGLESIAS, 2016).

In this work, the sediment transport and the medium-term morphological changes are numerically solved using the Delft3D model, considering the action of water waves

and tidal flow in Port of Portocel, located at Barra do Riacho, Aracruz, Espírito Santo State. Barra do Riacho's Port or Portocel is a port composed for seven berths that are utilized to woods and cellulose handling, ship parking, loading and landing operations and landing of wood in loose logs (LABTRANS, 2015). This port is near to the *Área de Proteção Ambiental Costa das Algas* (APA) environmental protection area and it is located at the north of the Jurong's shipyard.

In order to study seabed changes, a 2D validated numerical model with field data including measured currents and tidal elevations, seabed sediment composition, bed evolution, and waves is applied. The morphological seabed changes under water waves and tide effects in Portocel are simulated considering the morphological acceleration factor for a period of 20 years.

The objective of this work is to determine the morphological seabed changes with the focus to determine the rates of sedimentation and erosion in the Port of Portocel and surroundings. The morphological bed changes are modelled using the seabed sediment mass conservation equation (Exner equation) and the morphological acceleration factor method (LESSER *et al.*, 2004). The water flow is calculated using the mass and *momentum* conservation equations under Boussinesq approximation, and the wave propagation was described by the wave action density conservation equation. The van Rijn (2007) sediment transport formulation is applied to compute the bedload sediment transport under the effect of currents and waves.

2 OBJECTIVES

The overarching aim of this dissertation is to calculate and understand the physical processes involved in the medium-term morphological seabed changes in the Barra do Riacho's Port and surroundings.

2.1 SPECIFIC OBJECTIVES

- Study the hydrodynamic in Barra do Riacho's port and surroundings using the computational fluid dynamics technique.
- Study the water wave in Barra do Riacho's port and surroundings using computational fluid dynamics technique.
- Set up the morphological seabed changes in Barra do Riacho's port and surroundings using computational fluid dynamics technique.
- Understand the physical processes responsible for seabed changes during 20 years at the Barra do Riacho's port and surroundings.

3 LITERATURE REVIEW

In the coastal areas there is a demand to predict the morphological evolution of the seabed to propose strategies to maintain the depth of the navigation channels available for the transit of ships coming or leaving the port. The application of models based on computational fluid dynamics or statistical techniques is used to understand and forecast the morphological changes of the seabed. Nevertheless, both methods present limitations due to the long scale of time found in the physical processes of the morphodynamic evolution of the seabed.

However, the mathematical modeling of the physical problem based on the concept of "depth averaging" has facilitated the construction of specific models that allow the fast determination of the movement of water subjected to external force such as water waves, winds and friction with the seabed. Specific modeling was carried out to construct models for both the transport of sediments and the change of the seabed. These models working together have opened a window to expand the understanding and predict the long-term changes that occur on the seabed.

In next items the applications of numerical modelling in coastal areas and in *focus* on ports and harbours are presented.

3.1 MORPHOLOGICAL MODELLING

Numerical models and statistical analysis have been used to predict the morphological evolution of the seabed. The statistical models are suitable for seabed prediction over a long time scale, like in the study carried by Wijnberg and Terwindt (1995), who analyzed a coastal area portioned into different sliding form method, with a long time series, to obtain the changing trends. Years later, in East Anglian coast, Guillas et. al. (2011) used an Autoregressive Hilbertian (ARH) model to solve the long-term scale silting and scouring variation. This method enables a reduction of 10 % of the root to mean squared errors, leads to provide a basis for decision-making in port development.

Others authors studied the morphological evolution of the seabed based on GIS (Geographical Information System) and numerical analysis. For example, Wang et. al. (2014) applied this method to simulate the evolution and stability of the seabed in Yangshan Deep-Water Port. They evaluated the seabed before and after the construction of Yangshan Port and observed that before the construction of the port

the erosion and deposition variation was narrow, with values of 18,3 % and 28,0 %, respectively, and the stability was 53,7 %, characterizing relatively stable erosion and deposition character. After the construction, the erosion and deposition variation were 53,8 % and 23,4 %, respectively and the stability was 22,7 %, which showed more erosion than deposition in the port due to structures man-made which facilitated the seabed evolution more than natural evolution.

Numerical modelling is another common method to compute the seabed changes, in this case, the equations that describe the water flow (including waves), sediment transport and morphological seabed changes are solved using the Computational Fluid Dynamics (CFD) technique. There are three classes of morphological models that are used to represent the processes in some region: one-dimensional, two-dimensional and three-dimensional models.

One-dimensional models are used to represent the evolution of a profile in only one direction. Many authors utilized this kind of model to compute seabed profile evolution, for example, Cao et. al. (2004) developed a 1D shallow water hydrodynamics model to study the dam-break hydraulics over an erodible seabed. One of the results showed that over mobile beds, dam-break caused very active sediment exchange between the water column and the bed. Rakha et. al. (1997) combined phase-resolving wave transformation model with intra-wave sediment transport model to predict the sediment transport rates and the resulting in beach evolution. The results showed that the undertow contribution to the sediment transport rates is not dominating in all parts of the surf zone, even for eroding beaches, suggesting that other contributions should not be neglected.

The 1D models are used to solve depth-averaged *momentum* equations to calculate bed variations, as shown in Guo and Jin (1999) and Dongeren and Vriend (1994), in which obtained excellent agreement with the measured results.

In the 80's and 90's physical and mathematical modeling of wave and currents in two-dimensional space have advanced and modelling of wave and currents became possible. At the same time, the sediment transport formulations have been developed including the effect of currents and waves, which allow the use of coupled morphological models in coastal regions (VRIEND et. al., 1993). For example, Coeffe and Pechon (1982) developed a two-dimensional model, which calculates the longshore

currents, sediment transport and deduce the seabed evolution by the action of waves in a schematic semi-circular bay. This scheme provides results near the reality, which showed deposition in the left side of the bay due to the increasing of longshore transport and consequent erosion in the right side of the bay due to longshore transport reconstitution. The results showed that morphological evolution under action of waves and currents is not restricted to physics models and in this case, it only requires comparisons with real cases to prove the validity of the developed model.

In the last years, several researchers applied this kind of approach to simulate the morphological changes in coastal areas (DASTGHEIB et. al. (2008), Dissanayake et. al. (2009), Dissanayake et. al. (2012)). These studies presented the seabed morphological changes in Wadden Sea, obtaining as results a better understand of the tidal basins; the physical processes responsible to morphological features and the sedimentation patterns using Delft3D numerical model.

Other authors, as Ruggiero et. al. (2009), Ruggiero et. al. (2010) and Sivakholundu et. al. (2014) evaluated the morphological evolution in beaches using the hydrodynamics, waves, and sediment supply to predict the shoreline evolution with Delft3D depth-averaged (2DV) numerical model. The results showed that the morphological shoreline changes are associated with initial bathymetry; large events, such as El Niño and with cross-shore sediment transport. These aspects have an important role in shoreline morphological changes. A similar result was obtained by Vested et. al. (2013), who developed an empirical model to simulate the morphodynamics in Vilaine Estuary, France.

Xie et. al. (2013) and Wei and Wu (2014) made predictions in eastern coast of China using a depth-averaged numerical model (2DV). The first work reproduces the spatial sediment suspended concentration, the residual flow, the residual sediment transport and the sediment accumulation patterns in Hangzhou Bay. The results showed that the sediment accumulation takes place in the majority part of the bay and the tidal asymmetry pattern controls the sediment transport. While the second work, obtained results reliable to study area, which concluded that the Pearl River Delta is exhibiting filling up processes to form a delta plain in future.

Nowadays, the three-dimensional morphological model that considers the depthwise, specific mass and velocity variations, sediment concentration and others have been

applied to better understand the sediment transport and seabed evolution. Xu and You (2016) and Wang and Kang (2015) used a 3D numerical model to predict morphological changes in China in which showed that the morphological model results agreed well with the simulated values and the measured values. Also in China, Kuang et. al. (2013) used the Delft3D to study tidal flow, suspended sediment transport and bed evolution.

Ding et. al. (2006) developed a quasi-three-dimensional coastal area morphological model (Q3DCAM), which is composed by three submodels: irregular wave deformations, nearshore currents, and morphodynamics changes. This work was the first in literature to investigate the morphological processes model systematically considering the surface roller effect in the surf zone using the nonsinusoidal radiation stresses. The results showed that including 3D flow features the transport sediments onshore and offshore was improved, and the reproduction of seabed changes including coastal structures is capable to be simulated well, helping the support coastal sediment management and planning of practical coastal structures.

Gu et. al. (2016) investigated the wave condition and morphological variability on the evolution of double-sandbar system using quasi-three dimensional (3D) nearshore circulation model SHORECIRC and the SWAN wave model. The results showed that two main mechanisms were responsible for double-sandbar evolution: energetic waves and moderate waves. The first type determined the sandbar morphology and the second type was pronounced morphological crescentic pattern of sandbars.

3.2 SEABED EVOLUTION IN PORTS AND HARBOURS

In order to optimize the financial and time resources in the management of ports and harbors, the numerical modeling has been applied to predict the morphological seabed evolution. This method has been used in large cases involving ports, harbors and channels (MAYERLE et. al., 2015; LU and NAIRN, 2010; VAN MAREN et. al., 2015, GELFENBAUM et. al., 2003).

Wang et. al. (2014a) and Wang et. al. (2014b) used the FVCOM model to study the tidal discharges, flow asymmetries, and sediment discharges of three channels and perform one-hundred-year-long morphological simulation in construction of nuclear power plant and the expansion of Qinzhou Harbour, China together with the dredging

of the east navigational channel and model for investigating the tidal flow, sediment transport processes and 100-year morphological response of the channel-shoal system in Tieshan Port.

The models MIKE21, TK2D and IH-Dredge were ones of the models used to simulate the sediment dynamics, as shown in Vijverberg et. al. (2012) used the two-dimensional model MIKE21 to study the sediment dynamics in Lagos Harbour and the effects of local channel deepening in the Apapa area, that has a constant need to maintain the navigational channels at a defined depth. Shu-Hua et. al. (2009) used two-dimensional numerical model TK2D (“Tianke”) to simulate the tidal currents, sediment transport and seabed changes in Yangshan Deepwater Harbor and Alba et. al. (2014) used IH-Dredge three-dimensional numerical model to simulate the sediment transport and evolution of toxic substances in water and sediment in Port of Marin, Spain.

The Delft3D model has been applied successfully in many studies, as in Mayerle et. al. (2015) that used the Delft3D three-dimensional numerical model to investigate the sediment transport in navigation channel of the Paranagua Estuarine Complex, Brazil. Lu and Nairn (2010) used a three-dimensional hydrodynamic and sediment transport model to predict the morphological response of dredge pits, in this case, at a sand borrow pit located in Louisiana, USA. Van Maren et. al. (2015) studied the relative role of deepening and dredging on the sediment dynamics in the Ems Estuary. Gelfenbaum et. al. (2003) used the Delft3D model to simulate long-term morphological evolution in the Grays Harbor inlet.

Most recently, Prumm and Iglesias (2016) used two-dimensional process-based model Delft3D to simulate the hydrodynamics and sediment transport of an estuary before the port development and post-expansion. Three morphological factors were used corresponding to 3 different morphological times (1, 2 and 4 years). The results presented reasonable agreement with measured and computed data for velocities and water levels and a marked increase in sedimentation in the eastern part of the bank, leading to the infilling of the channel, that is crucial to operation the Port of Figueras and the shipyard. Furthermore, the development and the expansion of the port did not exert nonlocal impacts on estuarine environment.

Ying et. al. (2012) used two-dimensional numerical model Delft3D to simulate the hydrodynamics and sediment transport processes to analyze morphological changes in

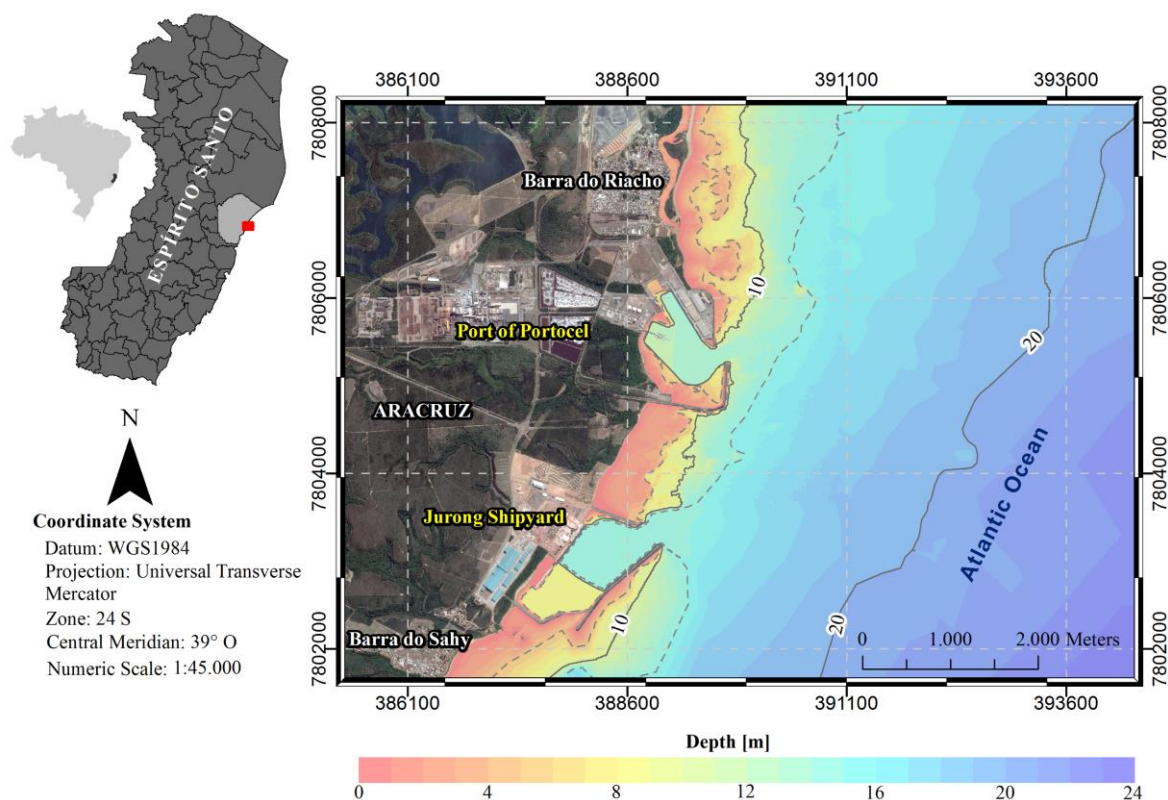
Yangshan Deepwater Harbor, China. The results showed that erosion and sedimentation patterns characterized the morphological changes, wherein sedimentation rates were highest in the first year and decreased in the next year. In addition, the sedimentation increased after 2007 but decreased after 2009. The routine dredging will be necessary to maintain the 15-m depth requirement for berths.

4 METODOLOGY

4.1 STUDY AREA

The Barra do Riacho's Port (Port of Portocel) shown in the Figure 4-1 is located at county of Aracruz, Barra do Riacho's district.

Figure 4-1 – Map showing the Barra do Riacho's Port and Jurong shipyard located in Aracruz, Brazil.



Source: Author

The Barra do Riacho's Port (Port of Portocel) is accessed by a 1,8 km road deviation from the main road (ES-010), a 46 km rail that connects the Piraque-açu station with the port and the maritime way from the ocean, located 60 km far from Vitória, ES.

The Barra do Riacho's port area is composed by two terminals: Barra do Riacho Waterway Terminal (TABR), which is Petrobras' property, and the other is the Terminal Especializado Portocel, that is Fibria and Cenibra's properties (LABTRANS, 2015).

The maneuvering basin is located within protection jetties with 460 m of diameter and depth of 11,8 m. The direction of the terminal's access channel is 065°, being 159 m

wide and 650 m long, measured from the beginning of the marked area to where it opens up to the jetties. The depth of the channel varies from a maximum of 13,5 m and a minimum of a 12,0 m (PORTOCEL, 2017).

4.2 HYDRODYNAMICS

4.2.1 Physical-mathematical model

To simulate the water movement, the Navier-Stokes equations to an incompressible fluid, considering shallow-water approximation and Boussinesq are solved. These equations do not have analytical solution, thereby, the equations are solved numerically. The currents and water levels are solved using the numerical solver of continuity and *momentum* equations, which directly affects the sediment transport and consequently the morphological seabed changes.

The system of equations consists of horizontal *momentum* equations (Eq. 1 and Eq. 2), the continuity equation (Eq. 3), the transport equation and a turbulence closure model. The vertical accelerations are small compared with the acceleration due to gravity which reduces the vertical *momentum* equation to the hydrostatic pressure relation.

$$\frac{\partial u}{\partial t} + u \frac{\partial u}{\partial x} + v \frac{\partial u}{\partial y} + \frac{\omega}{d + \eta} \frac{\partial u}{\partial \sigma} - fv = -\frac{1}{\rho} \frac{\partial p}{\partial x} + F_u + \frac{1}{(d + \eta)} \frac{\partial}{\partial \sigma} \left(\nu_v \frac{\partial u}{\partial \sigma} \right) \quad \text{Eq. 1}$$

$$\frac{\partial v}{\partial t} + u \frac{\partial v}{\partial x} + v \frac{\partial v}{\partial y} + \frac{\omega}{d + \eta} \frac{\partial v}{\partial \sigma} + fu = -\frac{1}{\rho} \frac{\partial p}{\partial y} + F_v + \frac{1}{(d + \eta)} \frac{\partial}{\partial \sigma} \left(\nu_v \frac{\partial v}{\partial \sigma} \right) \quad \text{Eq. 2}$$

In which d is the depth (meters); F_v and F_u are the horizontal Reynold's stresses (N/m²); u and v are the velocities components x, y (m/s); ρ is the specific water mass (kg/m³); f is the Coriolis parameter (1/s); ν is cinematic viscosity turbulent (m²/s); η is water level (m) and ω is the vertical velocity adapted to σ -coordinate system.

The vertical velocity ω adapted to σ -coordinate system is computed from continuity equation (GERRITSEN, *et. al.*, 2008).

$$\frac{\partial \eta}{\partial t} + \frac{\partial}{\partial x} [(d + \eta)u] + \frac{\partial}{\partial y} [(d + \eta)v] + \frac{\partial \omega}{\partial \sigma} = Q \quad \text{Eq. 3}$$

In which Q represents the external contributions due to precipitation (P), (q_{out} , q_{in}) is the local sources and sinks of water per unit (1/s), respectively; (E_{ev}) non-local sink due to evaporation, as shown below.

$$Q = h \int_{-1}^0 (q_{in} - q_{out}) d\sigma + P - E_{ev} \quad \text{Eq. 4}$$

The vertical velocity component w is relatively small and it can be expressed in Cartesian coordinate system (x, y, z) given in function of horizontal velocities, water level, depth and vertical velocity σ , as shown below:

$$w = \omega + u \left(\sigma \frac{\partial h}{\partial x} + \frac{\partial \eta}{\partial x} \right) + v \left(\sigma \frac{\partial h}{\partial y} + \frac{\partial \eta}{\partial y} \right) + \left(\sigma \frac{\partial h}{\partial t} + \frac{\partial \eta}{\partial t} \right) \quad \text{Eq. 5}$$

Under the shallow water assumption, the vertical *momentum* equation is reduced to a hydrostatic pressure equation. In this case, vertical accelerations due to buoyancy effects and sudden variations in the bottom topography are not considered (DELTARES, 2011), leading to:

$$\frac{\partial P}{\partial \sigma} = -g\rho H \quad \text{Eq. 6}$$

After integration, the hydrostatic pressure is given by:

$$P_z = P_o + g\rho_o(\eta - z) \quad \text{Eq. 7}$$

In which P_z is the pressure at the arbitrary level z ; P_o is the reference pressure; ρ_o is the background density and g is the gravity.

The Deflt3D numerical model is used to solve continuity and *momentum* equations. This model solves the unsteady shallow-water equations in two (depth-averaged) or three dimensions and the transport phenomena resulting from meteorological forces, including sediment transport and seabed evolution. The model uses the finite difference technique to numerically solve these equations.

Therefore, to obtain water levels and currents the equations 1, 2 and 4 will be utilized, in which the continuity (Eq. 4) will be responsible to estimate the water level and the other two equations will estimate the currents. To specify the processes in the studied

region, boundary conditions and initial conditions were used, which will be discussed later.

4.2.2 Model set up

4.2.2.1 Grid and bathymetry

The Barra do Riacho's port is numerically represented by a numerical grid in which the primary variables of flow, water level, and velocity, are solved on an Arakawa-C staggered grid (Figure 4-2-a).

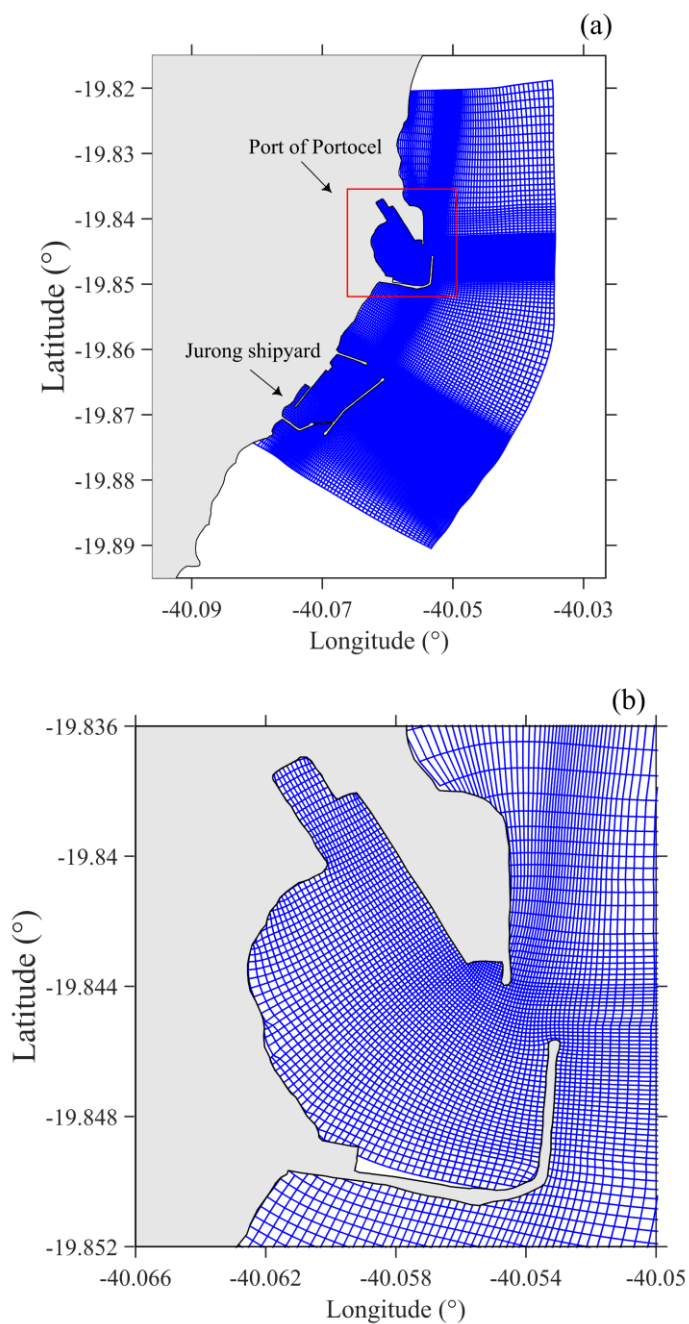
The grid has 17307 points, and its smaller grid size is 12 meters and the biggest grid size is approximately 100 meters. The grid is refined in the navigational channel to study in details the processes that occur into the port, as shown in the Figure 4-2-b.

The bathymetry was obtained through *in situ* measurements with multi and single beam echo sounder during the years of 2006, 2008, 2010 to 2012, 2014 and 2015, which were provided by Port of Portocel and nautical charts number 1420 and 142001 (bathymetry in the port is shown in the Figure 4-3. The Table 4-1 shows the details of the measured bathymetry data.

Table 4-1 – Bathymetry historical data.

Year	Type
2006	Eco Sounder Single Beam
2008	Eco Sounder Single Beam
2010	Eco Sounder Multi Beam
2011	Eco Sounder Multi Beam
2011	Eco Sounder Single Beam
2012	Eco Sounder Single Beam
2014	Eco Sounder Multi Beam
2014	Eco Sounder Multi Beam
2015	Eco Sounder Multi Beam

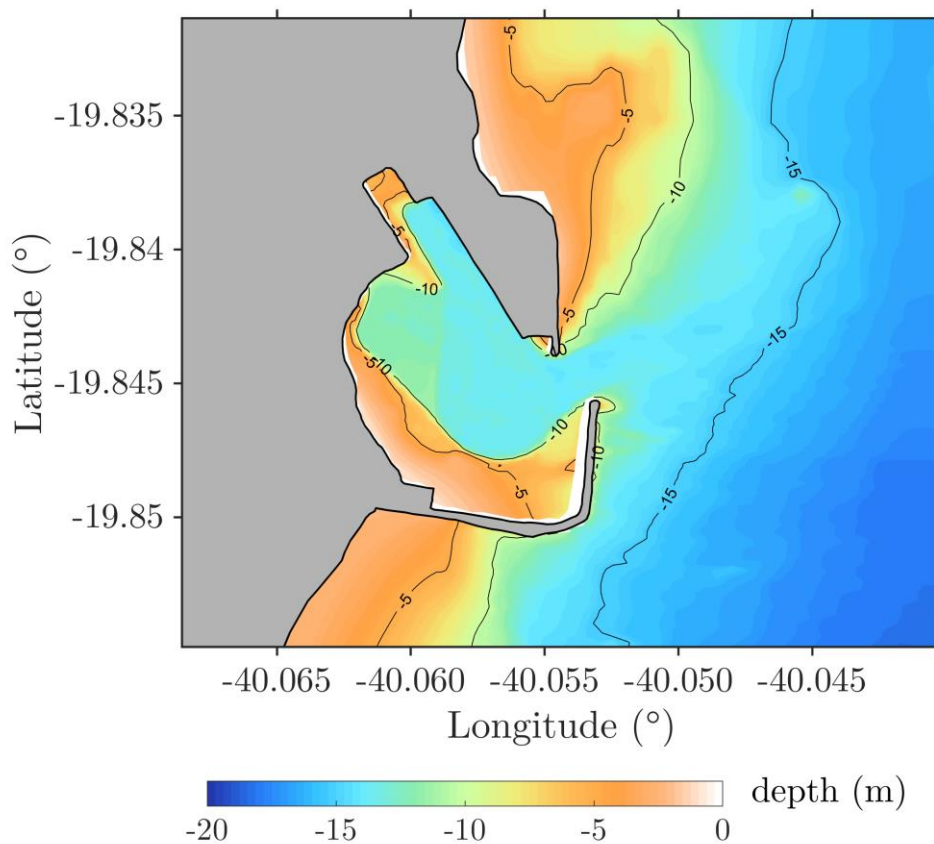
Figure 4-2 – Numerical grid used to represent hydro-morphological processes in Barra do Riacho's port, located at Barra do Riacho, Aracruz. In (a) the full grid and (b) a zoom at the Barra do Riacho's port.



Source: Author.

The currents and waves were measured during the year of 2009 using a current meter (ADCP – Acoustic Doppler Current Profiler) located at the $19^{\circ}50'57.74''S$ and $40^{\circ}02'44.89''W$ coordinates. Those data were obtained from the state environmental agency IEMA (Instituto Estadual de Meio Ambiente e Recursos Hídricos).

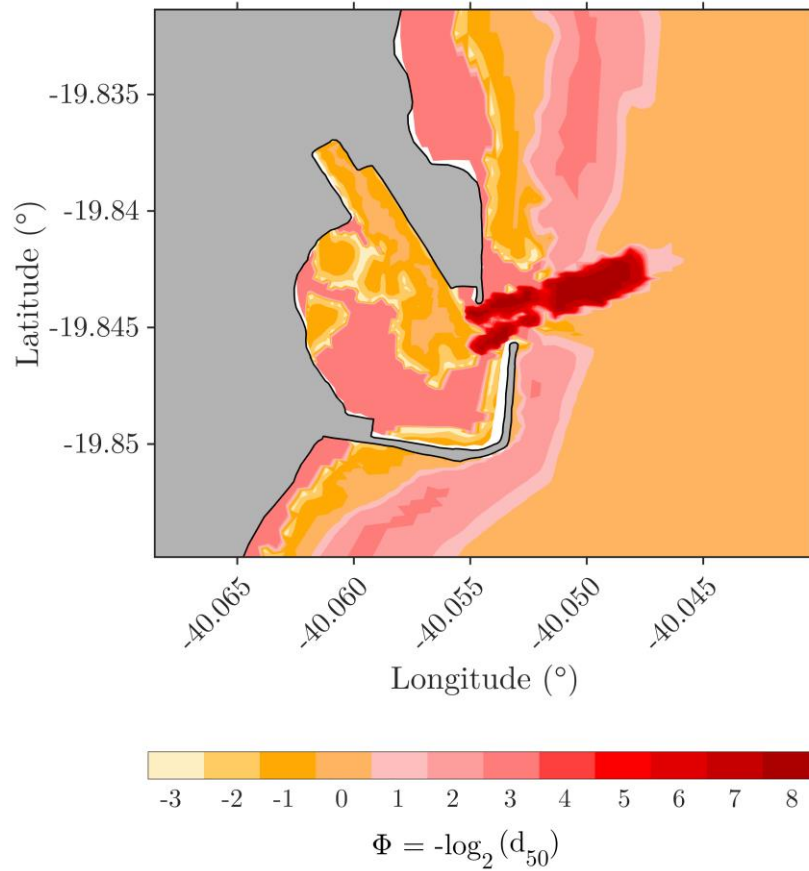
Figure 4-3 – Bathymetry provided by in situ measures and nautical charts digitalized for numerical grid.



Source: Author.

The tide was obtained from *in situ* measurements during 2014 and 2015-years using a tidal gauge. The seabed sediment composition (Figure 4-4) was compiled with measured data from Albino (1999), which studied the adjacent inner shelf from Vitória to Povoação beach. Besides, a geophysical study was conducted to identify the composition of the sediments in the Port of Portocel (provided by the Barra do Riacho's port).

Figure 4-4 – Sedimentological distribution interpolated for computational domain.



Source: Author.

4.2.2.2 Boundary and initial conditions

In order to solve the differential partial equations presented earlier, it was applied boundary conditions to specify the processes in study region. In this case, the σ coordinate system, the free surface ($\sigma = 0$) and bottom ($\sigma = -1$) are σ co-ordinate surfaces. The ω is the vertical velocity relative to the σ -plane. Thus, the impermeability of the surface and the bottom is considered by prescribing the following kinematic conditions:

$$\omega(\sigma = -1) = 0 \quad \omega(\sigma = 0) = 0 \quad \text{Eq. 8}$$

At the seabed, the boundary conditions applied are the bed stresses τ_{bx} e τ_{by} as function of the horizontal velocity gradient. The vertical diffusivity fluxes at free surface and at bed are considered null (RIJN and WALSTRA, 2003).

$$\frac{v_v}{h} \frac{\partial u}{\partial \sigma} \Big|_{\sigma=-1} = \frac{\tau_{bx}}{\rho} \quad \frac{v_v}{h} \frac{\partial v}{\partial \sigma} \Big|_{\sigma=-1} = \frac{\tau_{by}}{\rho} \quad \text{Eq. 9}$$

At the coast non-slip and impenetrability conditions are applied at the land boundaries. Riemann boundary conditions are applied to the open boundaries, which relates the boundary normal velocities and water level (VERBOOM and SLOB, 1984). The Riemann boundary conditions or Riemann invariants (R_i), are based on characteristics' method, in which the information of water level and normal velocity propagate through the characteristic curves. Riemann invariants are calculated following the relation: $R_i = U_\eta \pm \eta \sqrt{g/d}$, in which U_η is the normal velocity at the boundary and η is the water level. This boundary conditions was imposed at east, north and south boundaries using the tidal harmonics.

The initial conditions are cold start to water level and velocities, that is, the model begin with maximum water level and null velocities. Tidal elevations were calculated using the harmonics provided by TPXO Atlas tide inverse model solutions (EGBERT and EROFEEVA, 2002) at the open boundaries.

4.3 WAVES

4.3.1 Physical-mathematical model

The wave effects are included in the hydrodynamic model using a separated wave model. The wave model used in this study is the third-generation of SWAN (Simulating Waves Nearshore) model (HOLTHUIJSEN *et al.*, 1993).

The SWAN model computes the evolution of random, short-crested waves in coastal regions with deep, intermediate and shallow water ambient including currents or not. The SWAN model accounts for refractive propagation due to current and depth and represents the processes of wave generation by wind, dissipation due to whitecapping, bottom friction and depth-induced wave breaking and non-linear wave-wave interactions (both quadruplets and triads) (DELTARES, 2014).

In the SWAN model the waves are described through wave action density spectrum in a two-dimensional space, even if it is dominated by non-linear phenomenon, as surf zone (DELTARES, 2014). In this model, the spectrum evolution is described by the

spectral action balance equation, which is given in Cartesian coordinates, as shown below (Eq. 10):

$$\frac{\partial}{\partial t} N + \nabla_x \cdot [(\vec{c}_g + \vec{U}) N] + \frac{\partial}{\partial \sigma_f} c_\sigma N + \frac{\partial}{\partial \theta} c_\theta N = \frac{S}{\sigma_f} \quad \text{Eq. 11}$$

In which c_x and c_y are the wave phase velocities in geographic space x, y , respectively and c_θ and c_σ are the propagation velocities in spectral θ and σ_f space.

The left-hand side of the equation is the kinematic part of this equation. The second term denotes the propagation of wave energy in two-dimensional geographical \vec{x} -space, with the group velocity $\vec{c}_g = \partial \sigma_f / \partial \vec{k}$ following from the dispersion relation $\sigma_f^2 = g|\vec{k}| \tanh(|\vec{k}|d)$ where \vec{k} is the wave number vector and d the still water depth. The third term represents the effect of shifting the radian frequency due to variations in depth and mean currents. The fourth term represents depth- and refraction-induced currents. The quantities c_σ and c_θ are the propagation velocities in spectral space (σ_f, θ). The right-hand side contains S , which is the source/sink term that represents all physical processes which generate, dissipate, or redistribute wave energy (THE SWAN TEAM, 2016).

The wave radiation stresses result from the wave model used to update the stresses of hydrodynamic model and are calculated solving the action balance equation.

4.3.2 Model set up

4.3.2.1 Grid and bathymetry

The wave propagates from deep water to shallow water, where the study region is located. The spatial resolution of the grid in deep water is 100 meters, and to the domain of the study region the grid applied in hydrodynamic (Figure 4-2) is used to propagate the waves in coastal area. The information obtained from “father” grid (direction spectrum and frequencies) is given to boundary condition to “son” grid. For bathymetric representation of “father” grid was used data from GEBCO (available in <<http://www.gebco.net>>) and nautical charts.

4.3.2.2 Boundary and initial conditions

It was utilized the wave climatology in the study area from 40 years' ECMWF (*European Center for Medium-Range Weather Forecasts*) waves reanalysis in the oceanic region of the coast of Espírito Santo State. The data significant high, peak period and direction were the parameters used to input these data variables in the contours of the grid to validate in the period determined.

The module IHDATA-ONDA which is composed by a data bank denominated DOW (Downscaled Ocean Waves) obtained over 60 years (1948 – 2008) validated by satellites and buoys (IHCantabria, 2019), containing wave statistical parameters for the Brazilian coast was used simulate the wave climate and morphological evolution.

4.4 WAVE-CURRENT COUPLING

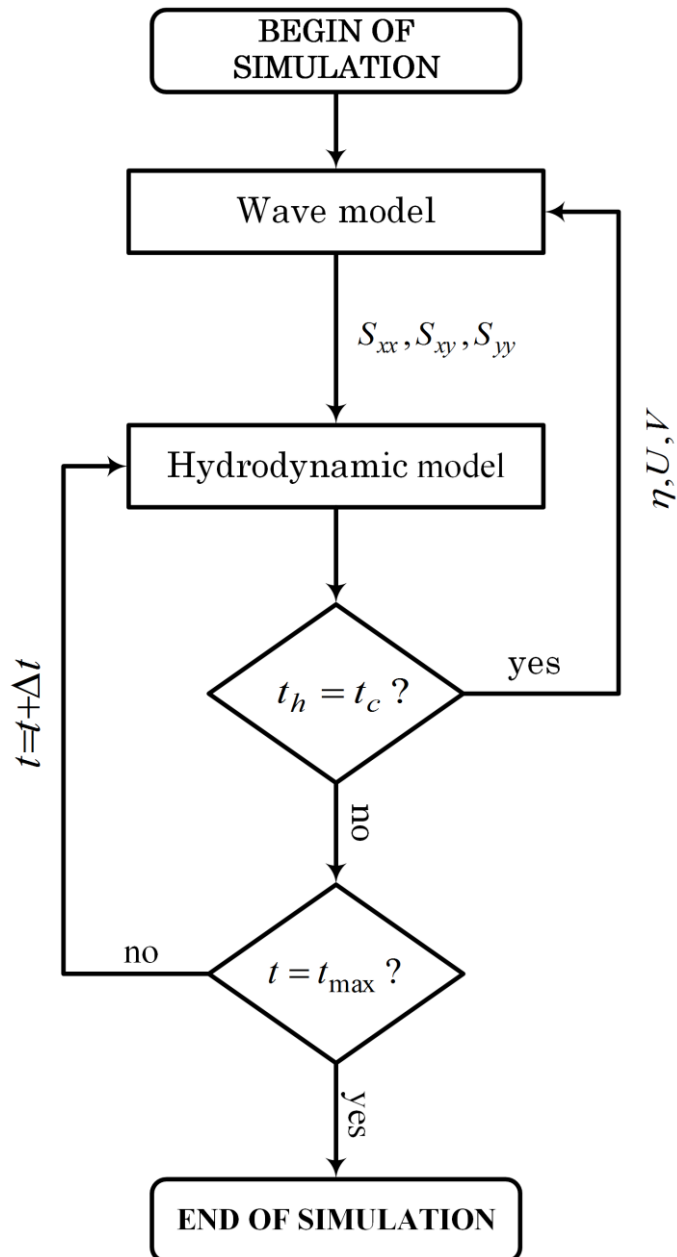
The wave-current interaction is a process that influences in the hydrodynamic and consequently in the sediment transport (KLEINHANS and GRASMEIJER, 2006). In order to better understand the sediment transport processes, the model is set considering both tidal induced currents and wave driven currents generated by wave radiation stress. For that, the hydrodynamic model and wave model are coupled, in other words, the radiation stresses generated by wave model (S_{xx}, S_{yy}, S_{xy} e S_{yx}) are converted to the hydrodynamic model (that calculate the water wave driven currents), and the results from the hydrodynamic model (η, U, V) are inputed in the wave model to account the wave-current interactions.

The coupling process begins when the currents and sea surface height calculated by hydrodynamic model are updated in the wave model. This information is used to calculate the wave-currents interactions and update the water level in the wave model. After the wave propagation computation, the new values of radiation stresses are set in the hydrodynamic model, in which the wave driven currents are calculated, as described by Lesser *et al.* (2004) and Lesser (2009).

In the wave-current coupling, the grid utilized to hydrodynamic simulation (Figure 4-2) and the grid utilized to wave simulation are coupled. In this case, while the hydrodynamic model is executed, the wave is considered steady until reach the coupling time.

The hydrodynamic model is executed for 20 minutes (coupling time) until the end of the simulation, in which the wave model is updated if the hydrodynamic simulation time (t_h) is equal to the coupling time (t_c). This process is presented below (Figure 4-5):

Figure 4-5 – Flowchart showing the coupling between the hydrodynamic and wave models.



Source: Author.

4.5 WIND

The wind used in this work is considered variable and was obtained from the ECMWF (European Centre for Medium-Range Weather Forecasts) Atmospheric Global Circulation data, which describes the dynamical evolution of the atmosphere

worldwide on the resolved scale and is used for medium-range, extended medium-range, and seasonal forecasts. The model uses the most accurate estimate of the current conditions and the most update description of the model physics and employs throughout modelled land surface conditions, ocean conditions, stratospheric representation and atmospheric dynamical processes (ECMWF, 2019).

4.6 SEDIMENT TRANSPORT AND SEABED EVOLUTION

The van Rijn (2007) sediment transport formulation is used in this work. In this formulation, the bedload and suspended sediment transport are divided in two components. The bedload sediment transport rate is given by the formula below (Eq. 12):

$$q_b = 0,015H \left(\frac{d_{50}}{H} \right)^{1,2} \left\{ \frac{U_e - U_{cr}}{[(s-1)gd_{50}]^{0,5}} \right\}^{1,5} \quad \text{Eq. 12}$$

In which q_b is the bedload sediment transport rate ($\text{m}^3/\text{m/s}$), d_{50} is mean diameter (m), H is the water column (m), s is the sediment specific gravity, U_e is the effective velocity (m/s), U_{cr} is the critical velocity (m/s).

The suspended sediment formula is given below:

$$q_s = 0,012U d_{50} D_*^{-0,6} \left\{ \frac{U_e - U_{cr}}{[(s-1)gd_{50}]^{0,5}} \right\}^{2,4} \quad \text{Eq. 13}$$

In which q_s is the suspended sediment transport rate ($\text{m}^3/\text{s/m}$), D_* is the dimensionless grain size and U is the mean current velocity in x, y (m/s).

As analyzed in Rosenhagen (2013), the Van Rijn (2007) formula is calibrated for coastal areas by influence of waves and currents, dominated by longshore currents. Besides, it's calibrated for regions with roughness and bed forms and in sediments with granulometric range 0.05 mm to 2 mm. Van Rijn (2007) consider the current velocities and orbital wave velocities calculated by hydrodynamic and wave models, which permit a better representation of the wave effects in sediment transport. Therefore, the critical velocity calculated by Van Rijn (2007) depends on roughness of sediment ($k_s = 2.5d_{50}$) and the orbital velocities, presented in regions influenced by waves, facilitates the begin of the sediment movement. The formula incorporates the

effect of waves in each grain size and wave period, that consists in calculate the sediment transport in each instant of wave cycle. Others formulas do not consider this kind of effect which promotes this formula the best option to this work.

The sediment map of the study region is obtained indirectly from side scan sonar measurements in 2014 provided by Portocel and *in situ* measured data from Albino (1999), who collected sediment samples in study area (compiled seabed sediment composition is shown the Figure 4-4).

In the North and South open boundaries, the Neumann boundary condition (zero gradient) is applied to sediment, while in the East boundary is adopted the Thatcher-Harleman condition (THATCHER and HARLEMAN, 1972). This condition is utilized to prevent the discontinuity in sediment concentrations, that occurs when flow change direction during the tidal cycle.

The seabed morphological evolution (EXNER, 1925) is calculated from the deposition (D) and erosion (E) rates, as well as the bed load rate transported in material volume by time unit (q_b), as shown in the equation below (Eq. 15):

$$(1 - \varepsilon) \frac{\partial z_b}{\partial t} = f_{morfac} \left(D - E + \frac{\partial q_b}{\partial x} + \frac{\partial q_b}{\partial y} \right) \quad \text{Eq. 14}$$

In which ε is the porosity and z_b the seabed height. The deposition and erosion rates are calculated from Ariathurai-Partheniades equations (PARTHENIADES, 1965; ARIATHURAI, 1974):

$$\left. \begin{aligned} E &= M_e \left(\frac{\tau}{\tau_{ce}} - 1 \right), \tau > \tau_{ce} \\ D &= w_s c \left(1 - \frac{\tau}{\tau_{cd}} \right), \tau < \tau_{cd} \end{aligned} \right\} \quad \text{Eq. 15}$$

In which M_e is the erosion parameter ($0,0002 \text{ kg/m}^2/\text{s}$), w_s is the settling velocity ($0,003 \text{ m/s}$), τ is the seabed stress due to currents, τ_{ce} ($0,5 \text{ N/m}^2$) e τ_{cd} (1000 N/m^2) are critical erosion and deposition stresses, respectively.

The morphological changes spend more time to happen that hydrodynamic changes, therefore the computational time to calculate the morphology is too long, since small

time steps (on the order of minutes and seconds) are used in the hydrodynamic simulations, making it impossible to simulate.

Therefore, the seabed morphological changes were calculated using a morphological acceleration factor f_{morph} (LESSER *et. al*, 2004; LESSER, 2009). This factor is used to help to deal with the difference between morphological and hydrodynamic times scales. It works multiplying the seabed sediment flux by a constant factor, thereby extending the morphological time step (Δt_{morph}), as shown below:

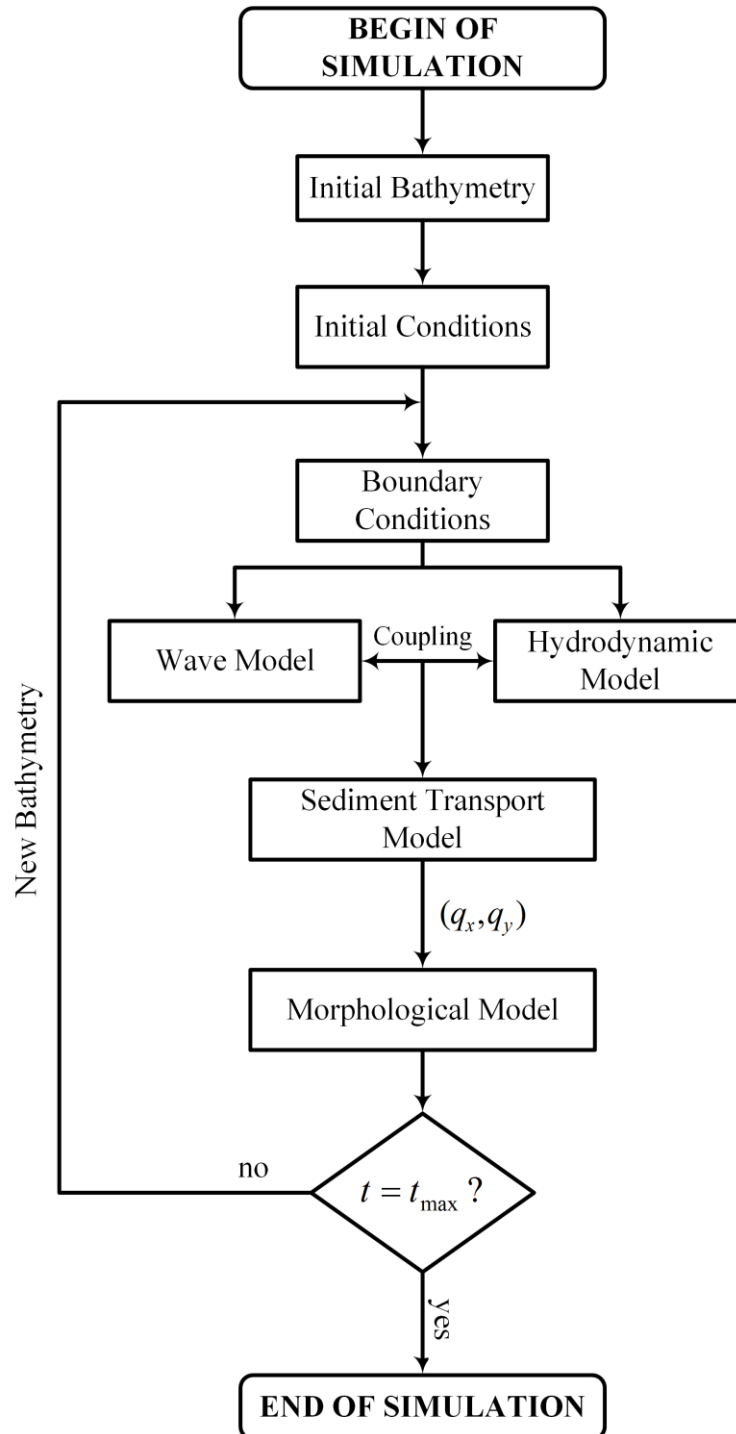
$$\Delta t_{morph} = f_{morph} \Delta t_{hydrodynamic} \quad \text{Eq. 16}$$

The morphological acceleration factor is calculated through the ratio between the morphological simulation time (e.g. 20 years), and the real simulation time in model (e.g. 1 year). The equation to calculate this factor is shown below:

$$f_{morph} = \frac{\text{Morphological simulation time}}{\text{Hydrodynamic simulated time}} \quad \text{Eq. 17}$$

The flowchart in the Figure 4-6 shows the interactions between waves, hydrodynamic, sediments transports, and morphological evolution models. From bathymetry, initial conditions of each model and boundary conditions, the wave and hydrodynamic model are initiated, being coupled at each 20 minutes. Thus, the sediment transport model is executed and the results are updated to the morphological evolution model, which update the bathymetry of hydrodynamic and wave models, repeating this cycle until reach the end of the simulation.

Figure 4-6 – Flowchart showing the interaction between wave, hydrodynamic, sediment transport and morphological evolution models.



Source: Author.

4.7 MODEL VALIDATION AND SCENARIOS

4.7.1 Model validation

The time series of velocities and waves are compared with *in situ* data collected using an ADCP (Acoustic Doppler Current Profiler) in 2009 located at the coordinates 19° 50' 57.74" S 40° 02' 44.89" W, in which the waves are measured hourly and the currents are measured with frequency of a half of an hour. The model results were analyzed using statistical parameters, as shown below (Table 4-2).

Table 4-2 – Statistics parameters and their meaning utilized in numerical model validation.

Statistic Parameter	Formulae	Meaning
d_r (WILLMOTT, 2012)	$\frac{\sum_{i=1}^n P_i - O_i }{c \sum_{i=1}^n O_i - \bar{O}_i }, \text{ if } \sum_{i=1}^n P_i - O_i \leq c \sum_{i=1}^n O_i - \bar{O}_i $ $\frac{c \sum_{i=1}^n O_i - \bar{O}_i }{\sum_{i=1}^n P_i - O_i } - 1, \text{ if } \sum_{i=1}^n P_i - O_i > c \sum_{i=1}^n O_i - \bar{O}_i $	Refined Willmott index of agreement. It is related to model accuracy.
d (WILLMOTT, 1985)	$d = 1 - \frac{\sum_{i=1}^n (P_i - O_i)^2}{\sum_{i=1}^n (P_i - \bar{P} + O_i - \bar{O})^2}$	Willmott index of agreement. It is related to model accuracy.
MAE	$\frac{1}{n} \sum_{i=1}^n P_i - O_i $	It's the average over the test sample of the absolute differences between prediction and actual observation where all individual differences have equal weight
$RMSE$	$\left(\frac{1}{n} \sum_{i=1}^n (P_i - O_i)^2 \right)^{1/2}$	It represents the square root of the second sample moment of the differences between predicted values and observed values. The RMSE serves to aggregate the magnitudes of the errors in predictions for various times into a single measure of predictive power
r	$\frac{\sum_{i=1}^n (P_i - \bar{P})(O_i - \bar{O})}{(n-1)\sigma_P\sigma_O}$	Coefficient of correlation

In which O is the measured data, P is the numerical model results, n is the number of observations, σ_P is the standard deviation of model results, σ_O is the standard deviation of measured data and c is a constant equal 2.

The measured bathymetry is compared with model results to validated the morphological evolution. The details of bathymetry are shown in Table 4-1.

4.7.2 Scenarios

The scenarios are used to verify the effect of morphological acceleration and morphological evolution. The scenarios are:

- Scenario 1: Wave validation

The wave model results are compared to measured data obtained from ADCP (Acoustic Doppler Current Profiler) in the year of 2009.

- Scenario 2: Hydrodynamic validation

The hydrodynamic model results from the spring and neap tide are compared with the measured data from ADCP (Acoustic Doppler Current Profiler) in the year of 2009. The hydrodynamic model is spun up for 15 days and the time step of 60 seconds.

- Scenario 3: Morphological evolution validation

The morphological model results were compared with bathymetry measured in 2010 and 2011.

- Scenario 4: Effect of morphological acceleration factor

The morphological changes are simulated including waves, wind, currents and sediment transport with and without morphological acceleration factor for 2 years. The morphological results are compared to morphological results using different f_{morfac} values (1, 30, 60 and 90).

- Scenario 5: Morphological evolution

The morphological changes are simulated including waves, currents and sediment transport with morphological acceleration factor of 20 years.

5 RESULTS AND DISCUSSION

5.1 MODELS VALIDATION

In this chapter data validation of the measured and Delft3D modelled results are described for the following parameters: waves, currents and morphological evolution. Model is compared against data measured in the 19° 50' 57.74"S and 40° 02' 44.89"W (WGS 84) coordinates in the proximities of the port of Portocel using an ADCP. Morphological evolution is validated using multibeam and singlebeam bathymetry measured in 2010 and 2011.

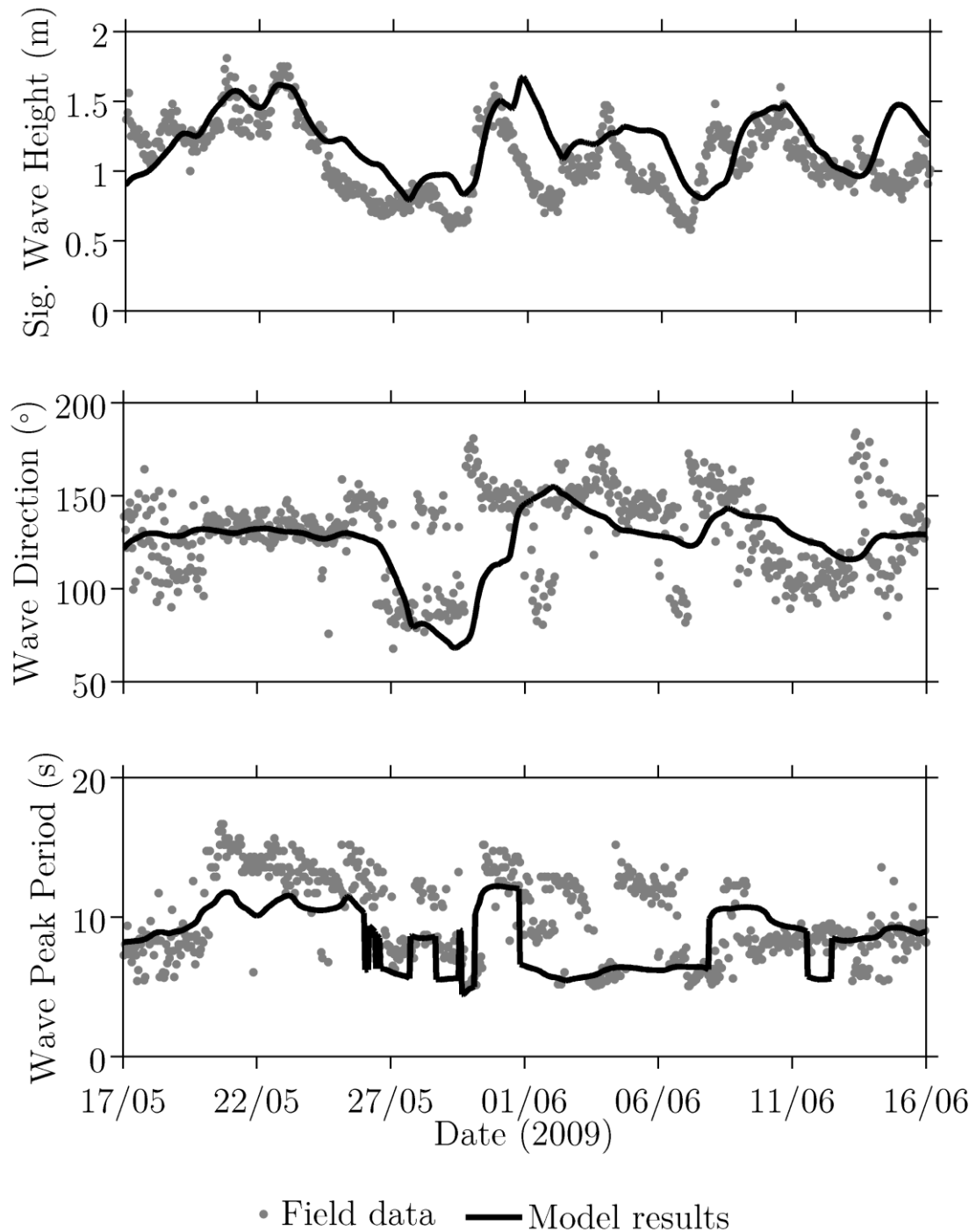
5.1.1 Wave modelling

The comparison between observed and modelled significant wave height, wave direction and wave peak period are shown in the Figure 5-1. The results showed a good agreement with measured data. The maximum significant wave height was found in May, with ~2 m and the minimum with ~0.6 m in June. The wave direction presented the mean direction of ~125° in May, the minimum (~70°) and the maximum of 170° in May. For wave peak period the minimum result was ~5 s and the maximum ~17s, both in May.

The underestimation observed in wave time series is widely known for SWAN simulations (LEE *et. al.*, 2010; ROGERS, HWANG, WANG, 2003; ALARI, RAUDSEPP, KÕUTST 2008; NOGUEIRA, 2010). Lee *et. al.* (2010) compared SWAN performance using two formulations for whitecapping, which is associated with the lag between modelled and observed data in time series. The Komen *et al.* (1984) formulation, also used in this work, underestimate the wave spectrum as well as the Alves and Banner (2003) formulation. Quantitatively, the Komen *et. al.* (1984) formulation underestimate 1 m for significant wave height and 0,6 s for wave peak period.

In general, the model was able to represent qualitatively and quantitatively the significant wave height, wave direction and wave peak period, which was possible to observed in time series shown in the Figure 5-1.

Figure 5-1 - Comparison of significant wave height, wave direction and wave peak period observed (dots) and modelled (solid line) during May 17 and June 16 of 2009.



Source: Author.

The statistical parameters for the measured and modelled wave data are shown in the Table 5-1. The significant wave height root mean square error (RMSE) value indicates reasonable margin of error (0.27 m), similar to others findings in literature, *e.g.*, Rusu, Pilar and Guedes (2008a) with 0.7 m, Padilha-Hernández *et. al.* (2007) found 0.51 m, Rusu, Pilar and Guedes (2008b) and Rusu *et. al.* (2011) with 0.3 m and the value found

by Lee *et. al.* (2010) of 0.4 m. The mean absolute error was 0.22 m. The two index of agreement ($d = 0.69$ and $d_r = 0.65$) indicates good agreement with modeled results, as well as correlation coefficient (r), 0.68 (Table 5-1). For direction, the root means square error (RMSE) also indicates congruent margin of error, that was 25.60° . This value as similar to found Nogueira (2010), 21.4° , lower than 30.30° found by Rusu, Pilar and Guedes (2008a) and Rusu *et. al.* (2011), 27.21° . The mean absolute error (MAE) for wave direction was 18.70° and the agreement index, d and d_r obtained was 0.57 and 0.52, respectively. The correlation coefficient for this case is 0.71.

For the wave peak period the RMSE value was 3.10 s which was similar to Curbani (2011), 3.53 s, upper to Rusu, Pilar and Guedes (2008a) with 2.03 s, Alves *et. al.* (2009), 2.27 s and Gorman *et. al.* (2003) with values of 1.66 s. The MAE was 2.90 s and the d and d_r were 0.54 and 0.51, respectively. The correlation error was 0.61 s.

In general, it can be seen that the simulations are in good agreement with the measurements.

Table 5-1 – Statistical parameters in terms of significant wave height (H_s), wave direction and wave peak period (T_p).

Wave parameter	MAE	RMSE	d	dr	r
Hs	0.22m	0.27m	0.69	0.65	0.68
Direction	18.70°	25.60°	0.57	0.52	0.71
Tp	2.90s	3.10s	0.54	0.51	0.61

5.1.2 Hydrodynamic modelling

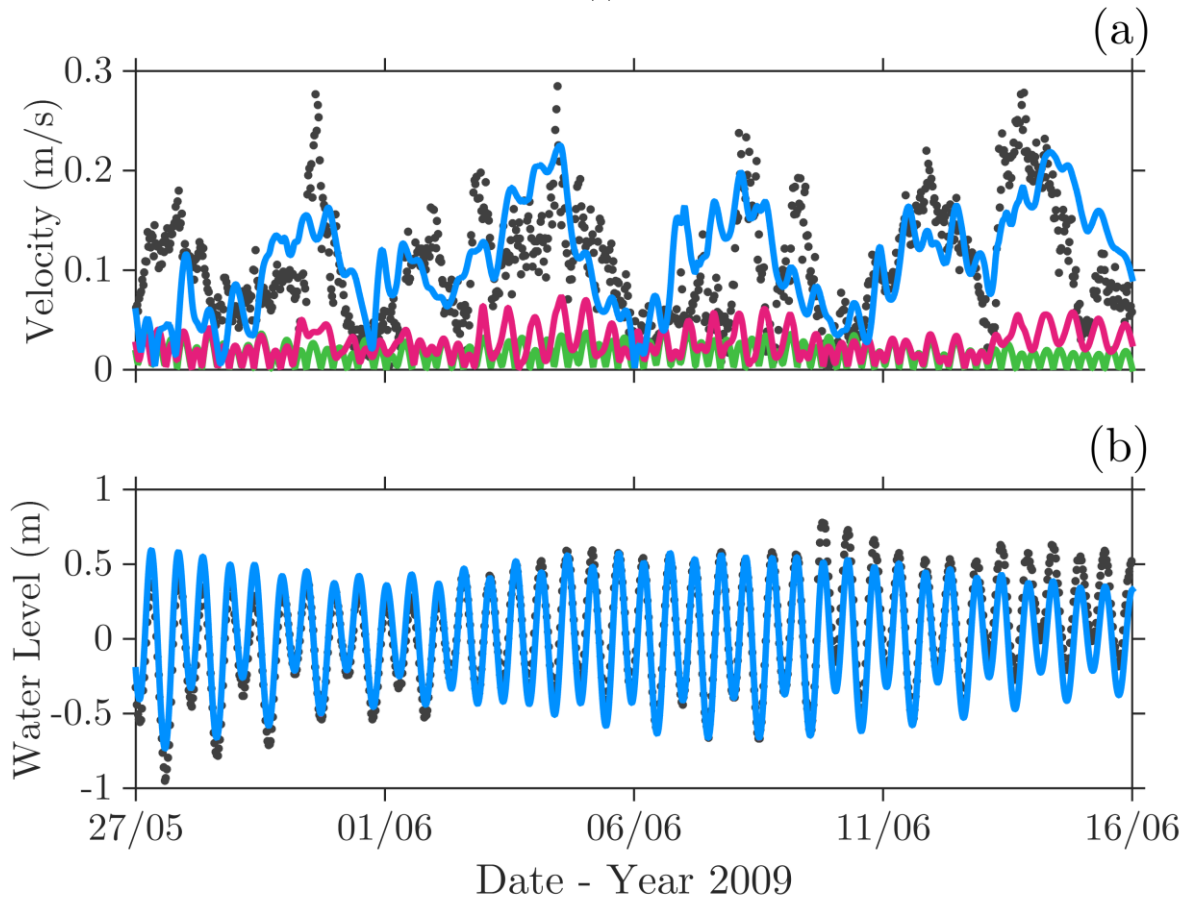
The Figure 5-2 shows the comparison between velocities considering tide, tide and wind and tide, wind and wave calculated by hydrodynamic model with observed data and the water level for the same conditions.

The results in the Figure 5-2.a shown that the wave is the main mechanism that drive velocity variations, since both tidal and wind generated velocities are too weak compared with the former. Comparison between tidal, wind and waves driven currents shown a reasonable agreement with measured data. The maximum modelled velocity (considering tide, wind and waves) was 0.22 m/s and the minimum was 0.001 m/s. The maximum observed data was 0.28 m/s and the minimum was 0.004 m/s.

The water level is shown in the Figure 5-2.b, it is possible to observe that the measured data and modelled have similar behavior. The maximum modelled and observed water

levels are 0.55 m and 0.77 m, respectively. Therefore, this difference can be correlated to meteorological effect not account in this work, that could match the observed and modelled data.

Figure 5-2 - Comparison of velocities considering tide (green line), tide and wind (magenta line) and tide, wind and wave (blue line) with observed data (black dots) in (a). Same for water levels in (b).



• Observed — Tide — Tide and Wind — Tide, Wind and Wave

Source: Author.

Tide is the main mechanism that drive water level changes in the study area, since local wind and waves have minor influence on water level fluctuations, as observed in the Figure 5-2.b. Overlapped lines in the Figure 5-2.b show no observable differences between tide and wind with tide, wind and wave modelled results. These results show a good agreement with the observed data for water level. The maximum observed was 0.93 m and the maximum modelled was 0.72 m. Table 5-2 show the statistical parameters comparing measured and modelled results for currents and water levels.

Statistical results shown a good accuracy of model results. For velocities the highest correlation coefficients are found when tide, wind and wave are considered ($r = 0.65$),

in which the minor RMSE (0.04 m/s) and MAE (0.05 m/s) are also found. A good agreement is found for water levels for all simulations considered (TWW, TW and T), with $r > 0.9$ for all simulations and lower RMSE (<0.1256) and MAE (<0.1779).

Table 5-2 – Statistics parameters for measured and modelled velocities and water levels.

	Simulation	d	d_r	RMSE	MAE	r	r^2
Velocity	TWW*	0.62	0.53	0.04 m/s	0.05 m/s	0.65	0.43
	TW*	0.4479	0.1453	0.0939 m/s	0.132 m/s	0.094	0.0093
	T*	0.4227	0.0441	0.1061 m/s	0.1571 m/s	0.0316	0.001
Water Level	TWW*	0.9664	0.8309	0.1241 m	0.1734 m	0.9365	0.877
	TW*	0.9658	0.8297	0.1255 m	0.1779 m	0.9262	0.8761
	T*	0.9657	0.8296	0.1256 m	0.1772 m	0.9361	.8762

*TWW – Tide, Wind and Wave, TW – Tide and Wind; T – Tide only.

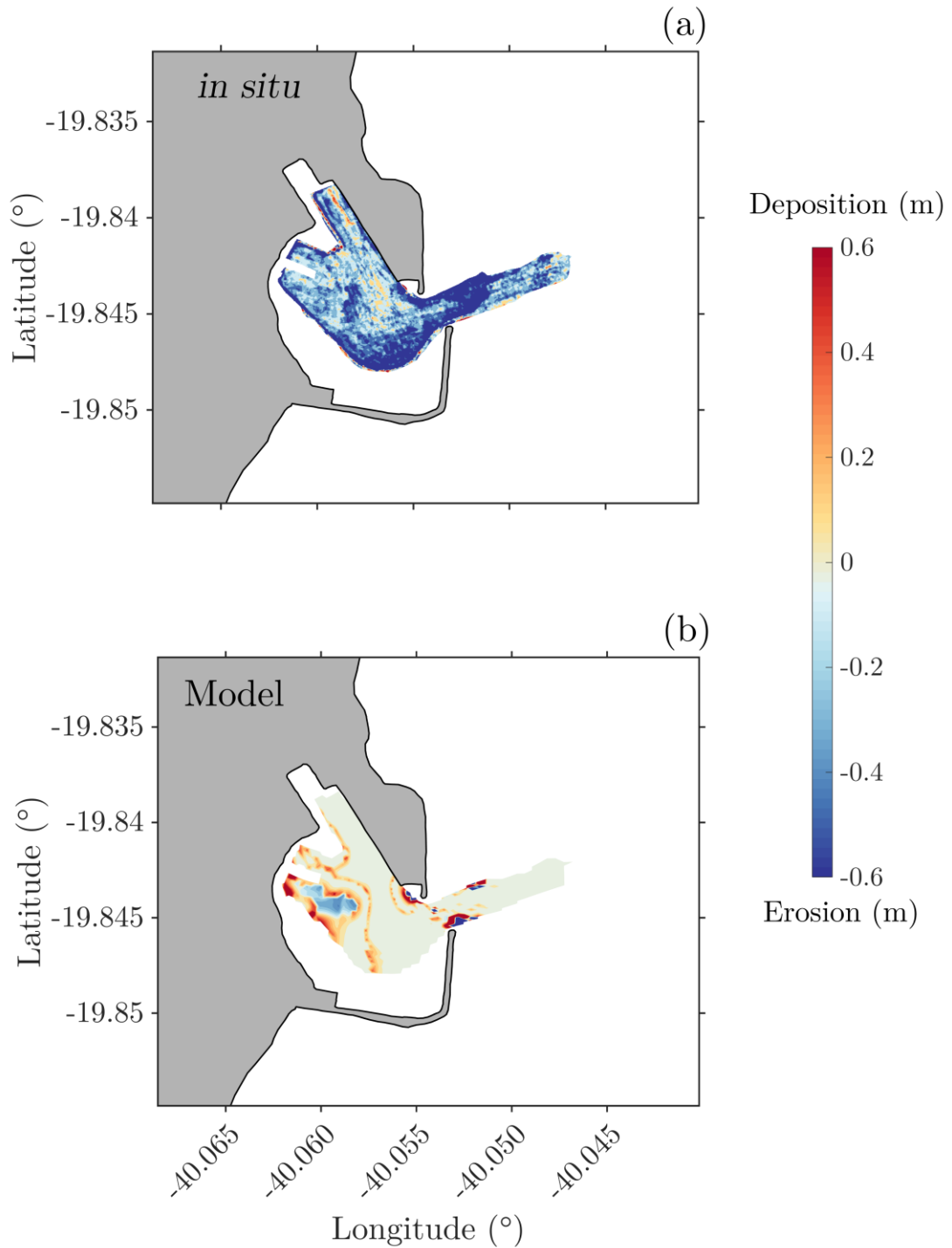
5.1.3 Morphological modelling

To validate the morphological model 1 year of data was utilized (2010-2011) and make one map bathymetric which represents the net morphological bed changes between 2011 and 2010 (Figure 5-3).

Comparing modelled (Figure 5-3.b) and in situ (Figure 5-3.a) measured data it is possible to observed that erosion and deposition areas have the same order of magnitude. The inner part of the channel is observed in measured data deposition zones in order of 0.4 m. Near extremity of the entrance of the navigation channel is also noted deposition areas as registered in model results.

The difference observed in measured and modelled results may be associated with the grid size resolution. Even using a grid size about 12m in the port, some abrupt seabed slopes may not be properly represented in the model. The lack of information of high-resolution seabed sediment composition also lead to an underestimation of the bedload and suspended sediment transport rates and consequently the erosion and deposition patterns.

Figure 5-3 – Morphological net changes in situ (a) and modelled (b) in port of Portocel for 1 year (2010 – 2011).



Source: Author.

5.2 THE WAVE CLIMATOLOGY

The wave climatology was simulated using the SWAN model with 60 years reanalysis data from the DOW database. Results showing the wave propagation at the port are shown below:

- Direction (D)

Table 5-3 shows the statistics of directions, peak period and significant wave heights of waves in Port of Portocel obtained from DOW database in the -39.9928°W and -19.8681°S coordinates. The results from DOW were used to propagate the waves and analyze the predominant waves in study area. Six classes of wave direction are observed: ENE, E, ESE, SE, SSE and S. These results in the study area shown that 90% of waves come from the ESE and SE direction ($110^{\circ} - 130^{\circ}$), as shown in the Table 5-3. This finding is also observed when analyzing the number of occurrences and energy spectrum as shown in the histogram of directions and the energy spectrum for H_s and T_p as function of direction. (Figure 5-4.a and Figure 5-4.b).

Table 5-3 – Statistics wave parameters in study region from 1948 to 2008 from DOW database.

Direction	Direction's Probability	Peak period (s)			Significant wave height (m)		
		$T_{p50\%}$	$T_{p90\%}$	$T_{p99\%}$	$H_{s50\%}$	$H_{s90\%}$	$H_{s99\%}$
ENE	0.30%	7.31	7.57	7.62	0.61	0.79	0.81
E	3.26%	7.19	8.71	9.92	1.10	1.47	1.95
ESE	60.05%	7.17	9.27	11.18	1.49	2.03	2.51
SE	30.08%	9.08	11.86	13.59	1.64	2.22	2.76
SSE	6.21%	11.00	13.56	14.93	1.83	2.52	3.17
S	0.10%	11.06	13.16	14.66	1.89	2.83	3.51

- Peak period (s)

The wave statistics for wave peak period to characterize the wave climate in Port of Portocel is shown in Table 5-3.

The mode of distribution is presented in the histogram (Figure 5-4.c) between 6,0 and 8,0s. About 60% of waves came from ESE direction with 7s o peak period. The percentile 90% and 99% for the ESE direction shown 9.27s and 11.18s, respectively.

The joint distribution of T_p as function of direction show that ‘the most waves in study area is came from T_p typical of ESE direction (5 – 9s). The analysis of T_p and H_s shown that the T_p typical is represented for waves between 1 – 2 m of H_s (Figure 5-4.d).

- Significant wave height (m)

The statistics for significant wave height to characterize the wave climate in Port of Portocel is shown in Table 5-3. The most of the wave energy in the spectrum is concentrate between 1.30 – 1.70 m (Figure 5-4.e) which is observed the most of number of occurrences. The median is 1.49 m and the percentiles 90% and 99% are 2.03 m and

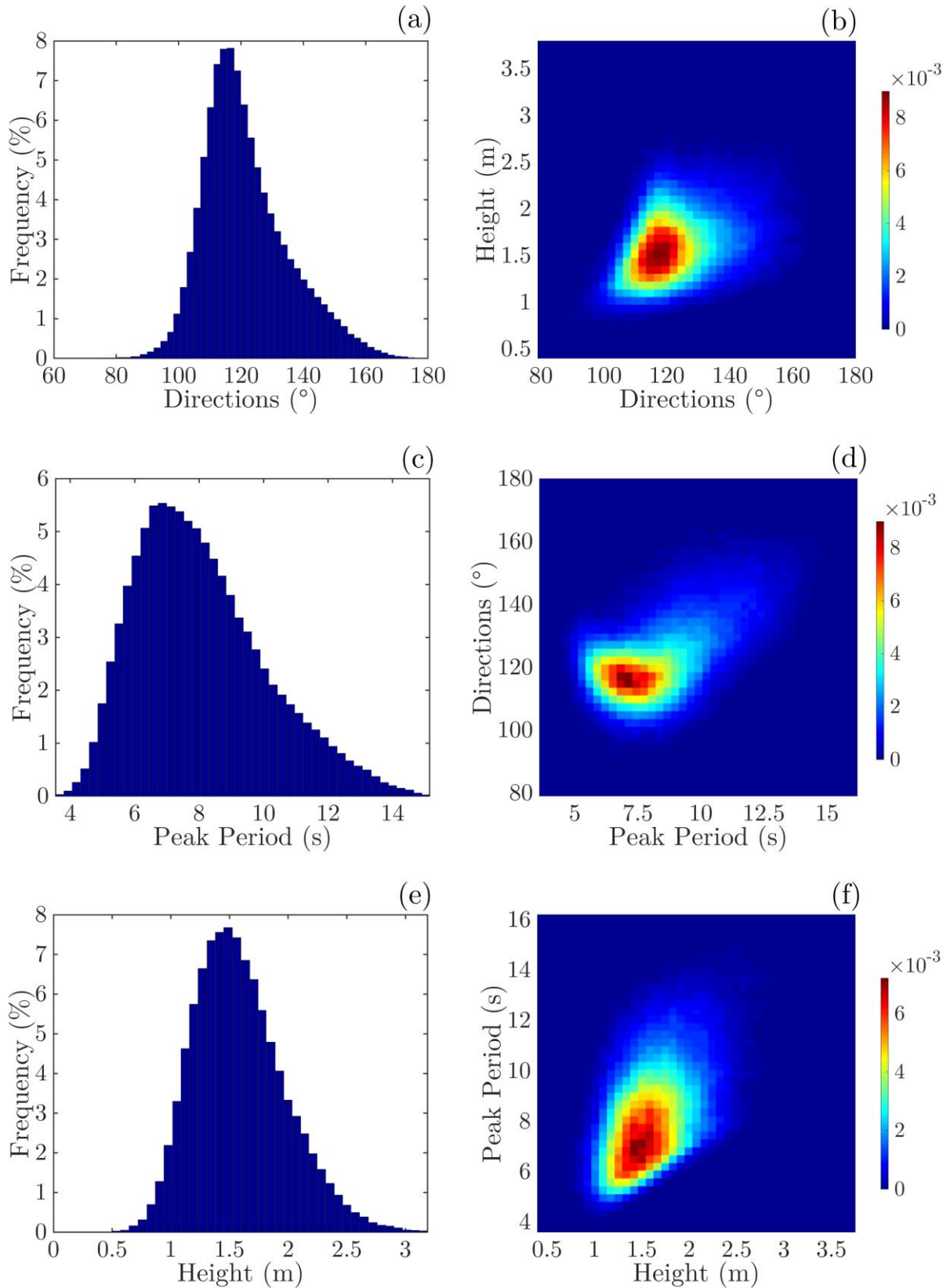
2.51 m for ESE direction. It is important to note that it was not found significant wave height greater than 3.50 m and lower than 0.50 m.

The joint distribution of H_s as function of direction (Figure 5-4.b) show that the typical H_s occurred in the most typical directions of waves ($105^\circ - 135^\circ$). For H_s as function of T_s is characterized for waves with T_p varying between 5 and 10s, with the peak occurring in 7s (Figure 5-4.f).

The Figure 5-5 shows the significant wave height (H_s) and directions found in the Port of Portocel and surroundings. Figure 5-5. (a) and (b) shows the waves in ENE and E directions with significant wave heights between 1 and 2 m. These waves reach the inner part of Port of Portocel with heights of 0.75 – 1 m. The Figure 5-5 (c) and (d) shows the wave significant height in ESE and SE directions, respectively. The significant wave height is higher than that observed for ENE and E directions. In this case wave heights up to 0.75 m are found inside the Port of Portocel and 2.5 m outside the port (Figure 5-5.c). For E direction (Figure 5-5.d) the wave significant height come lesser than ENE, E and ESE directions, reaching 1 m inside Port of Portocel and 2.75 m in outside part. The SSE and S (Figure 5-5.e and Figure 5-5.g, respectively) directions are represented for the highest wave significant height in outer part of the port that reach up to 3.50 m in some regions outside the port. The inner part of the port is characterized for small waves, mainly, in S direction, that the predominant wave significant height was lower than 0.25 m.

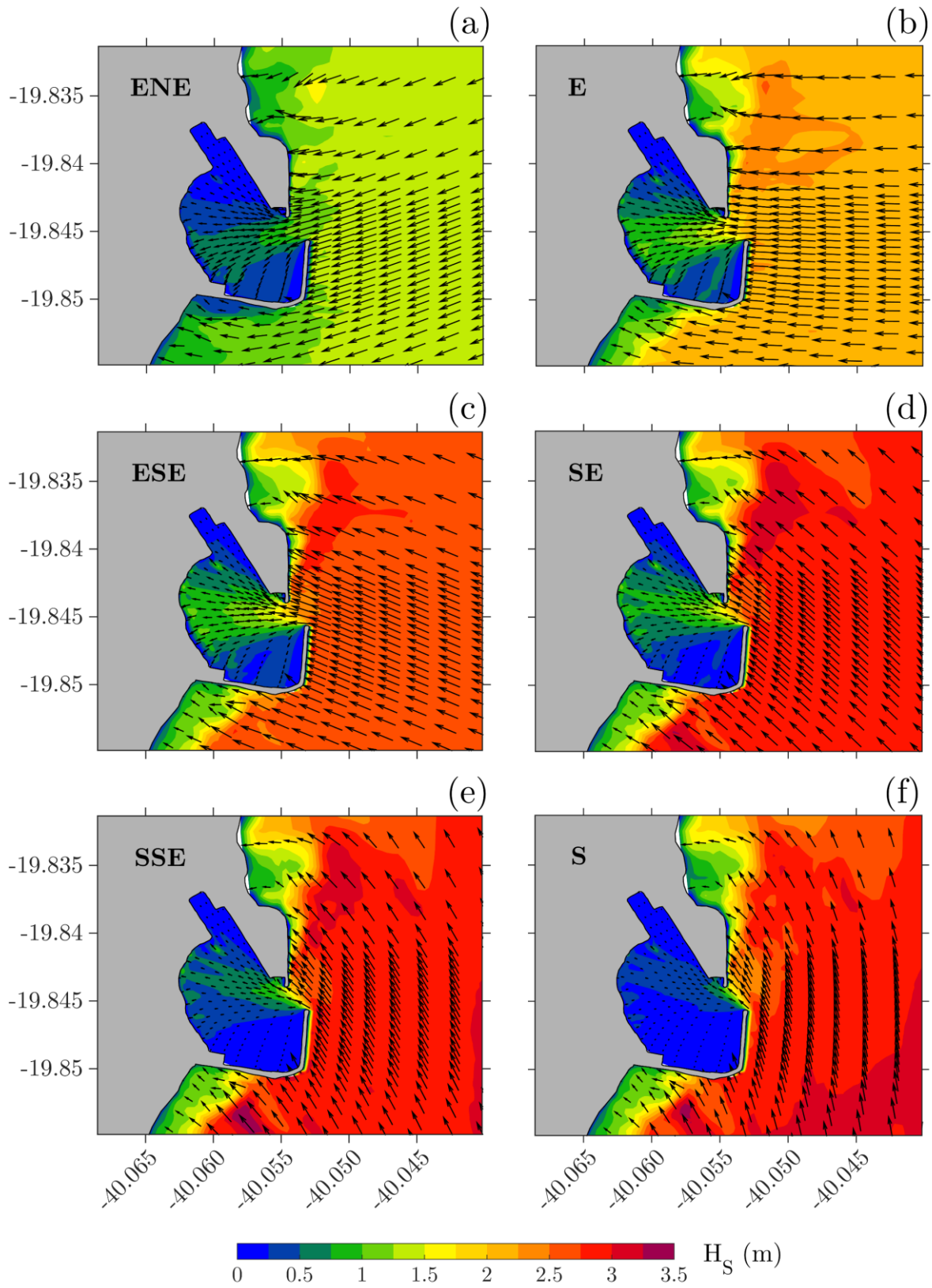
It noticeable that the waves coming from the E, ESE and SE directions reach the inner part of the port with the highest wave heights (0.75 – 1 m inside the port), even with presence of the port's sheltering structure blocks most of the waves coming these directions.

Figure 5-4 – Histogram of direction (a), peak period (c) and wave height (e) and energy spectrum of directions x wave height (b), peak period x direction (d) and wave height x peak period (f) in port of Portocel. Data source: SMC-DOW.



Source: author.

Figure 5-5 – Significant wave height (m) distribution and mean direction of wave propagation using 60 years SMC climatology data as boundary conditions.



5.3 THE HYDRODYNAMICS

The hydrodynamic and wave models were set to generate currents to the sediment transport model input considering the effects of tide, wave and wind. The period modelled was selected by harmonic forecast generated by FEMAR (2000) harmonics, in which was obtained a time series where the minor and larger neap and spring tide was chosen. The spring tide was chosen because it represents the higher velocities.

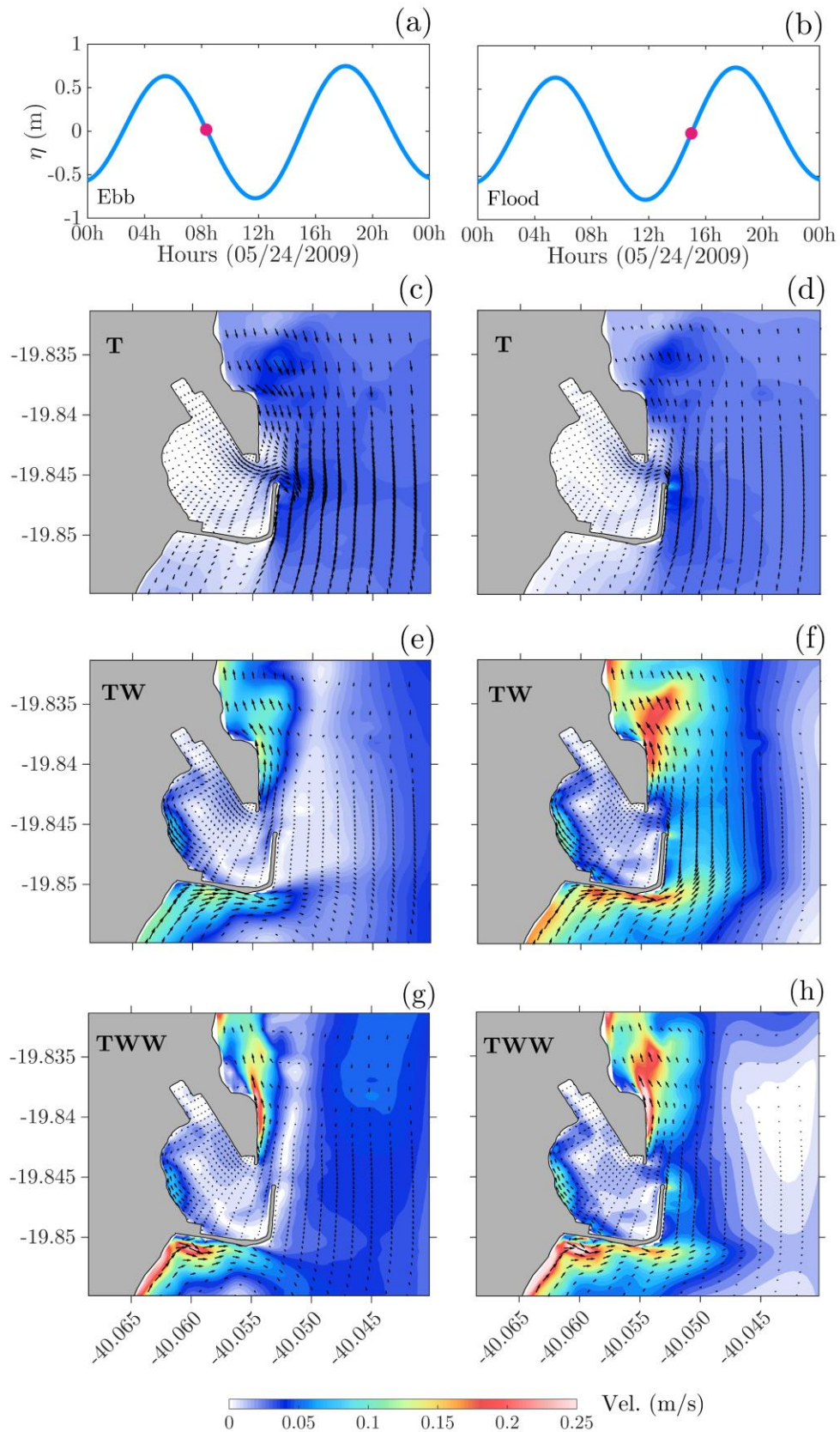
Tidal heights and velocities are shown in the Figure 5-6. Tidal elevations in Figure 5-6.a and b represent the ebb and flood levels respectively.

As observed in the Figure 5-6 the Port of Portocel seems to be dominated by ebb currents, it's possible to realized it in the Figure 5-6.c where the magnitude of ebb current is bigger than flood currents (shown in the Figure 5-6.d), as shown in the vector map of ebb currents (Figure 5-6.c). The Figure 5-6.c and d represents the tide driven currents, the Figure 5-6.e and f represents the tide and wind currents and the Figure 5-6.g and g represents the tide, wind and wave currents.

In the Figure 5-6.e and f it's possible to observe the effect of the wind on tidal currents for the ebb and flood periods. The maximum velocities are higher outside of the port wherein the wind effect is particularly noticeable, when the longshore littoral current is most visible. The maximum current velocity was about 0.2 m/s in north and south part of port during flood tide period, while the minimum was registered inside the port during ebb tide conditions with approximately 0.075 m/s. The longshore current observed here was generated by current induced by wind stress. It's also possible to note a cyclonic eddy inside the basin channel in comparison with Figure 5-6.c and d (tide only currents).

Figure 5-6.g and h show the influence of tide, wind and wave in ebb and flood tide periods, respectively. The maximum velocity is 0.25 m/s in ebb and flood periods located outside of the basin, while the maximum velocities inner the basin was found mainly reaching about 0.75 m/s in flood and 0.175 m/s in ebb. The minimum velocity is 0.05 m/s at the inner basin and north of the port. The highest velocities are found mainly in flood periods, north and south of the port, while inside of the basin is possible to notice a presence of a cyclonic eddy, that with lower velocities.

Figure 5-6 - Velocities in ebb and flood tidal currents. The figures a and b represent tidal levels in ebb and flood, respectively. The figures c, e and g represent tide only, tide and wind and tide, wind and wave, respectively in ebb cycle and the figures d, and h are tide only, tide and wind and tide, wind and wave, respectively in flood cycle.



Source: author.

The results show the influence of sea waves in the longshore currents, that can be a major transport agent, mainly by stirring sediment by orbital motion, and they can give rise to net currents and residual transport, e.g. longshore currents (WANG, 1995). When waves break at surf zone, they release a large part of their energy and they transform into momentum to the water column. The effect of these waves can be observed by the presence of waves currents that can increase the flow velocity when the waves and currents are in the same direction or can also decrease the flow velocity when are in opposite direction. This way, the waves and curenets effects are highly affected by the influence of waves and currents direction (JIA, *et. al.*, 2015).

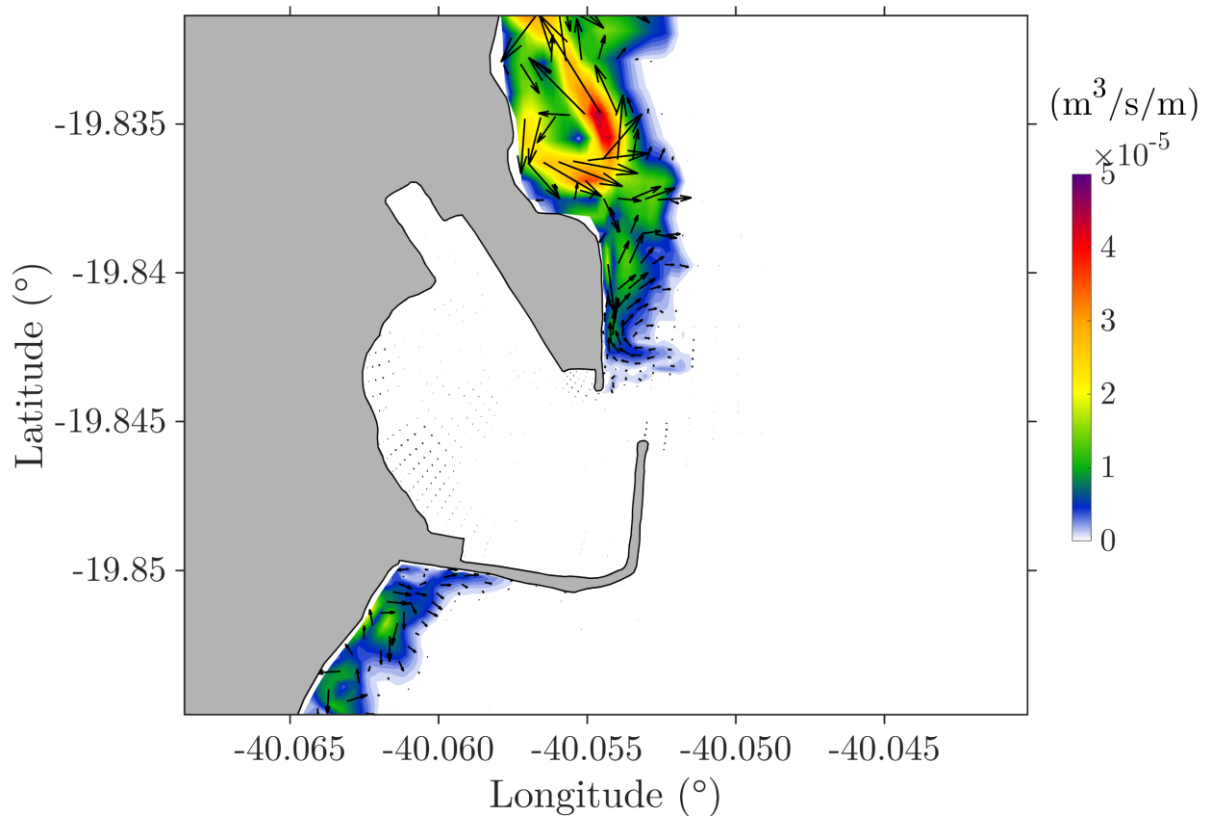
The currents generated by wind and waves flow parallel to the shoreline and they may contribute to hydrodynamic in Port of Portocel basin and consequently in the sediment transport, which will be discussed hereafter.

5.4 SEDIMENT TRANSPORT

The sediment transport in Port of Portocel is computed from the flow velocities considering the effect of tidal flow including wind and waves. The flow, morphodynamic and wave models were validated and discussed earlier.

The net bedload and suspended sediment transport rates integrated in twelve tide periods in spring tide conditions with wave climatology (ESE were the main direction) are shown in the Figure 5-7 and Figure 5-8, respectively. The suspended sediment transport rate is located alongshore the coast, as shown in the Figure 5-7, mainly in north part where sediment transport rates of $4.5 \times 10^{-5} \text{ m}^3/\text{s}/\text{m}$ are found near to an anticyclonic eddy and lower rates in south part of the port, which reached magnitudes of $1 \times 10^{-5} \text{ m}^3/\text{s}/\text{m}$. Inside the port, it is observed very low suspended sediment transport rates. In this case, the net suspended sediment transport has northward direction, following the same flow direction (Figure 5-6).

Figure 5-7: Net suspended sediment transport rate in Port of Portocel and surroundings.

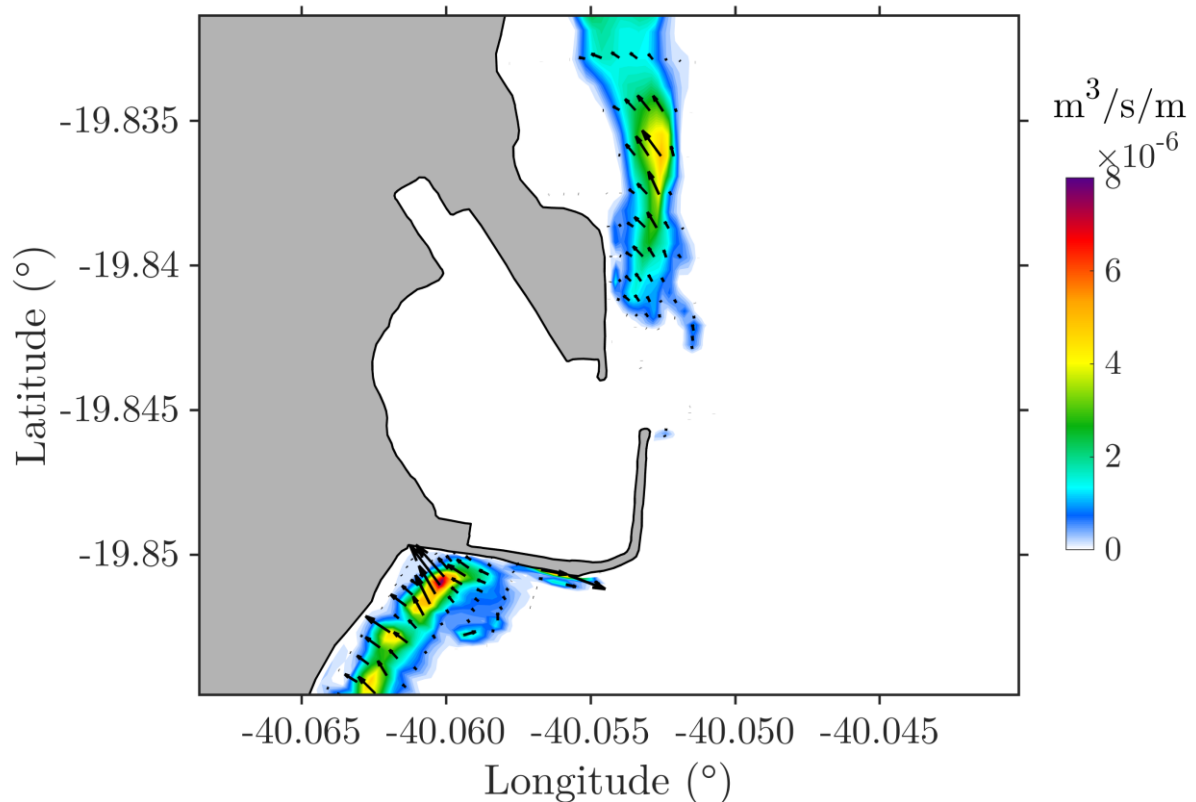


Source: author.

Net bedload sediment concentration during spring tide conditions are concentrated in south of the port (magnitudes as higher as $8 \times 10^{-6} \text{ m}^3/\text{s}/\text{m}$) and the north portion of the port (magnitudes of $4 \times 10^{-6} \text{ m}^3/\text{s}/\text{m}$), as shown in the Figure 5-8. It is important to observe that there is no significant bedload sediment transport inside the port of Portocel and most of the sediment transport is found outside of berth. The residual sediment transport rate has a strong correlation with the currents induced by wave and tidal flow in flood tide conditions probably due to the wave stirring (KLEINHANS & GRASMEIJER, 2006), wave asymmetry, longitudinal currents (CAYOCCA, 2001) and the wave turbulence (LESSER *et al.*, 2004).

Coupled wave and tidal forces work effectively to mobilize the sediment, as opposed to the tide only simulations. The waves approaching to the coast are refracted by sea bathymetry, so the wave begins to reduce its speed due to the friction of the particles with the bottom, and this is accompanied by the increase of its height and subsequently cause the wave break. The wave break generates strong currents and forces that leads to the resuspension of sediments and the longitudinal and transverse sediment transport.

Figure 5-8 – Net bedload sediment transport rate in the Port of Portocel and surroundings.



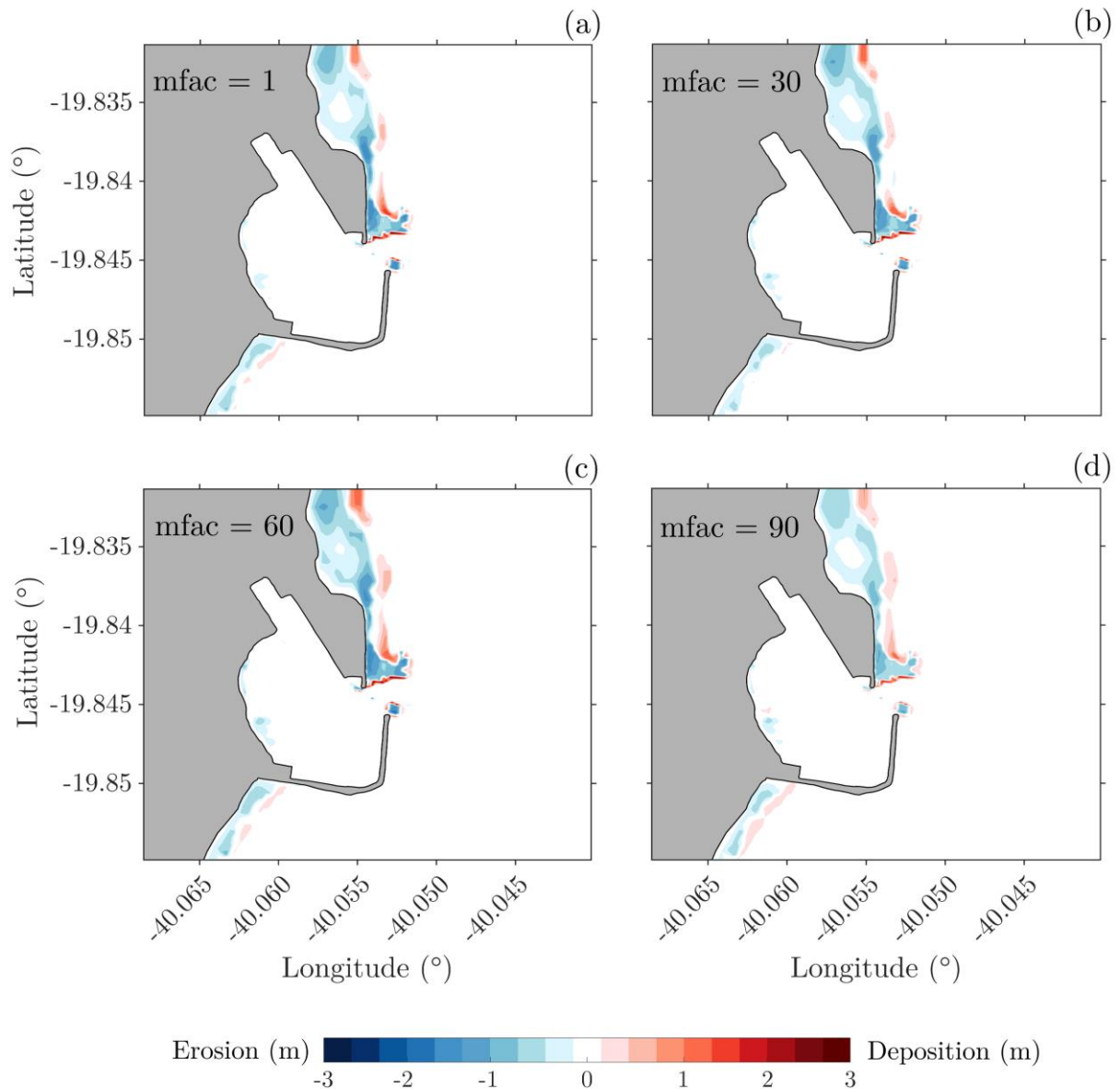
Source: Author.

5.5 MORPHOLOGICAL EVOLUTION

The morphological changes are simulated in terms of Morfac. As discussed by Dissanayake (2012), there is no specific highest value for Morfac at the present, therefore, a sensitivity analysis was made to know the most suitable Morfac is better to apply, which is, determine the best safety value to apply in this analysis. In this case four Morfac (1, 30, 60 and 90) were set to show the stability of the different Morfac values applied.

Figure 5-9 shows the morphological evolution under four Morfac approaches for a period of 2 years. Erosion and sedimentation of port of Portocel was estimated for four Morfac approaches. The results show that both Morfac (1, 30, 60, and 90) tend to show similar variation in sedimentation and erosion changes in seabed level. Dissanayake (2012) in Ley Bay also observed similar results using Morfac 30 and 60, while Lesser (2004) also concluded that the comparison between different morphological factor shows no discernible differences.

Figure 5-9 – Predicted bathymetries under different Morfac value 1 (a), 30 (b), 60 (c) and 90 (d).



Source: Author.

The simulation with a Morfac = 1 is considered as the benchmark simulation. The resulting morphology of the benchmark case was compared with Morfac 30, 60 and 90. It was observed that the erosion and deposition patterns inside and outside the port is similar using Morfac 30, 60 and 90. These results show that Morfac = 90 generates erosion and depositions patterns very close to the another Morfacs and therefore may be used to study the morphological evolution accelerating morphological changes to 20 years.

Medium-term morphological evolutions in the port of Portocel for 1, 2.5, 5, 10, 15 and 20 years are shown in Figure 5-10. The results for 1 year (Figure 5-10.a) shows erosion region in north of port of Portocel that reached 0,66 m while deposition located

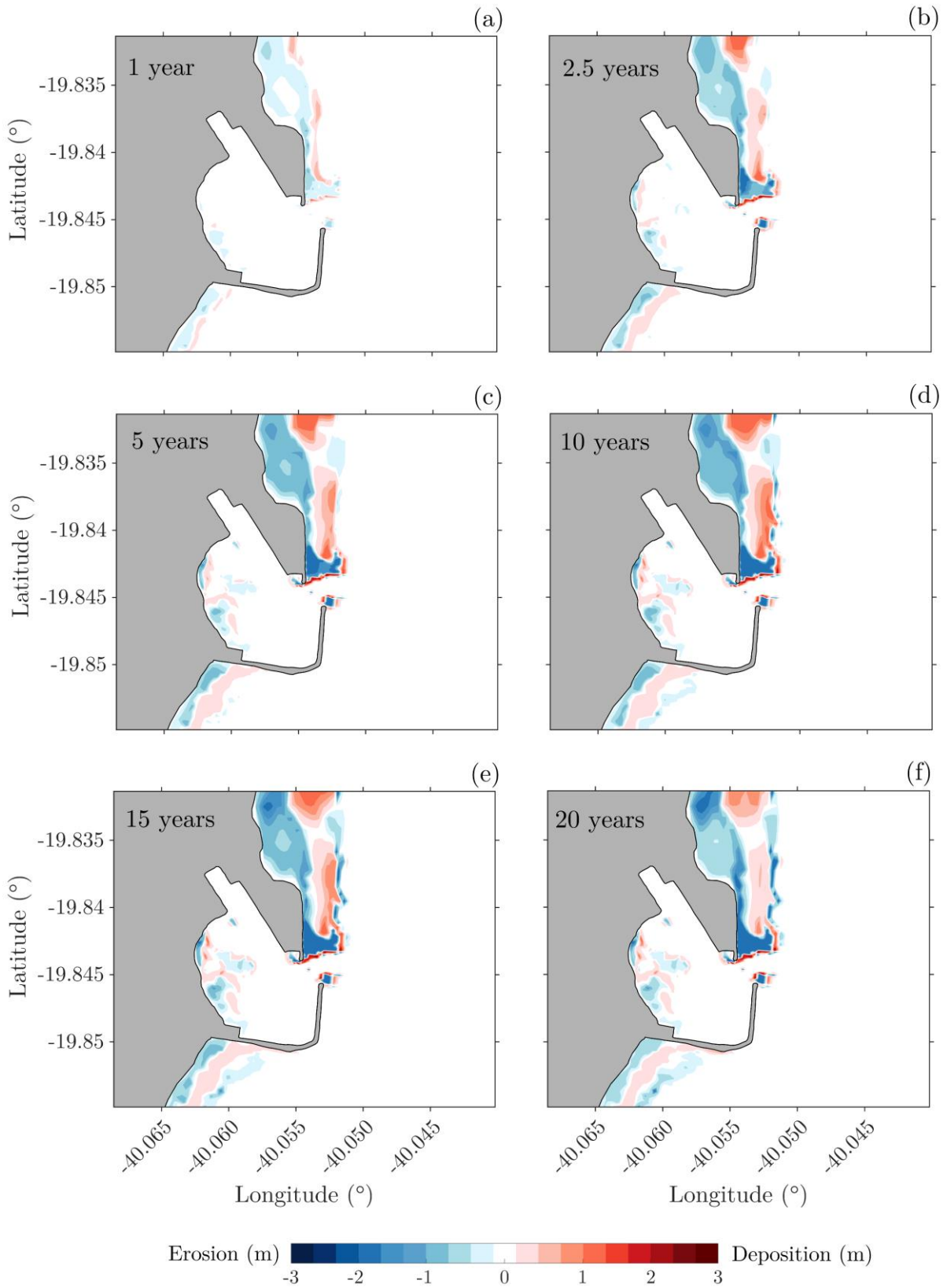
adjacent of the port reached 0,66 m. Inside the port an erosion and deposition areas are found with seabed changes of 0,33 m each. From 2.5 years to 20 years it was observed the intensification of erosion e deposition patterns and the arising of deposition areas inside the port, which reached 1,33 m both. In the north region of the port of Portocel erosion and the deposition rates reached 2,00 m and 2,33 m, respectively. In the south portion of the port erosion and deposition areas appeared ranging from 1 m (erosion) to 0,33 m (deposition), as shown in the Figure 5-10.f. In the end of 20 years the erosion regions were compensated by large submerged sandbars built by combination of waves, tide and wind effect, similar behavior is also found by Cayocca (2001).

It was observed that the greater net sediment transport is related with zones where the bigger morphological bed level changes are found. The north region of the port has the highest sediment transport rates, same location where the highest erosion and deposition areas were found. The erosion areas, located near the coast, are related to longshore current. These currents can drive sediment of the shallower areas to deep areas building large sandbars, which is also observed in Coutinho (2015) and Silva *et. al.* (2013). The last author shown that the coast where the port is located has a regressive behavior.

The presence of a sheltered area inside the port prevented the waves that propagates from ESE direction to reach the inner parts of the port. These waves dissipate most of its energy at the groyne that creates a shadow zone where high erosion and deposition areas can be found. In the absence of the effect of waves inside the port, this region experiences lower morphological bed level changes in comparison with the north region outside the port.

The extremity of both sides of navigation channel, the highest velocities and sediment transport rates were found as shown in the Figure 5-6, Figure 5-7 and Figure 5-8. These areas are where the waves dissipate its energy and where tidal currents are higher due to the mass conservation in shallow depths. Those are the main physical processes that contribute to the higher erosion and deposition rates found in the extremity of entrance of the navigation channel. Furthermore, the lateritic ferruginous breastplates are not considered for the simulation, which may contribute in the sedimentation and erosion patterns in port of Portocel and surroundings.

Figure 5-10 – Morphological evolution in port of Portocel using Morfac = 90 for 1 year (a), 2.5 years (b), 5 years (c), 10 years (d), 15 years (e) and 20 years (f). Blue is erosion patterns and red is the deposition patterns.



Source: Author.

Seabed sediment composition has very low resolution in the model due to lack of measurements, which lead to constant values over some regions in the model. According to Xie *et. al.* (2013) the net sediment transport and consequently the morphological evolution in a cohesive sediment environment can be controlled by the asymmetry of the tide. The main mechanism for cohesive sediment transport is tidal asymmetry. This author pointed that the deformation of tidal wave during its propagation shows that if the top is faster than the trough of wave causes flood dominance and when trough is faster generates ebb dominance leading to an asymmetry in tidal currents. In this work, morphological evolution is simulated in a non-cohesive sediment environment.

The results suggest that the main mechanism for sediment transport is wave currents which act resuspending the sediment and the longshore currents that drive the sediment transport and consequently the morphological changes. Tide is a secondary mechanism, once its currents are too weak to transport sediments. In this case tidal elevations change the locations where the wave breaks, it is important mainly near to the coast north and south of the port where the lower depths and bed slopes are found.

The morphological changes may be interfered by the presence of rivers as shown in Coutinho (2015). The presence of Riacho's river in north of port of Portocel might interfere in the sedimentation and erosion patterns due to the contribution of suspended sediment inside and near the port areas. However, river contribution is not taken into account due to the lack of data, like, sediment discharge, flow and sediment distribution. It's important to be pointed out that there are no studies about Riacho's river to inform the fate and dispersion of its plume.

The currents generated by the wind and wave systems drives preferably the sediment from shallow waters to deep waters as seen in Figure 5-7 and Figure 5-8. According to Albino *et. al.* (2006) the wind and wave systems are responsible for the variations and inversions of magnitude and direction of longshore currents. The currents that drive sediment transport may be associate with the erosion which is observed, mainly, adjacent of the coast in study region in north, south and inside of port (Figure 5-10).

As observed in the hydrodynamics (Figure 5-6), the presence of waves and wind are the two main agents that affects the hydrodynamic and consequently the morphological changes. Wave driven currents have northward direction (Figure 5-6),

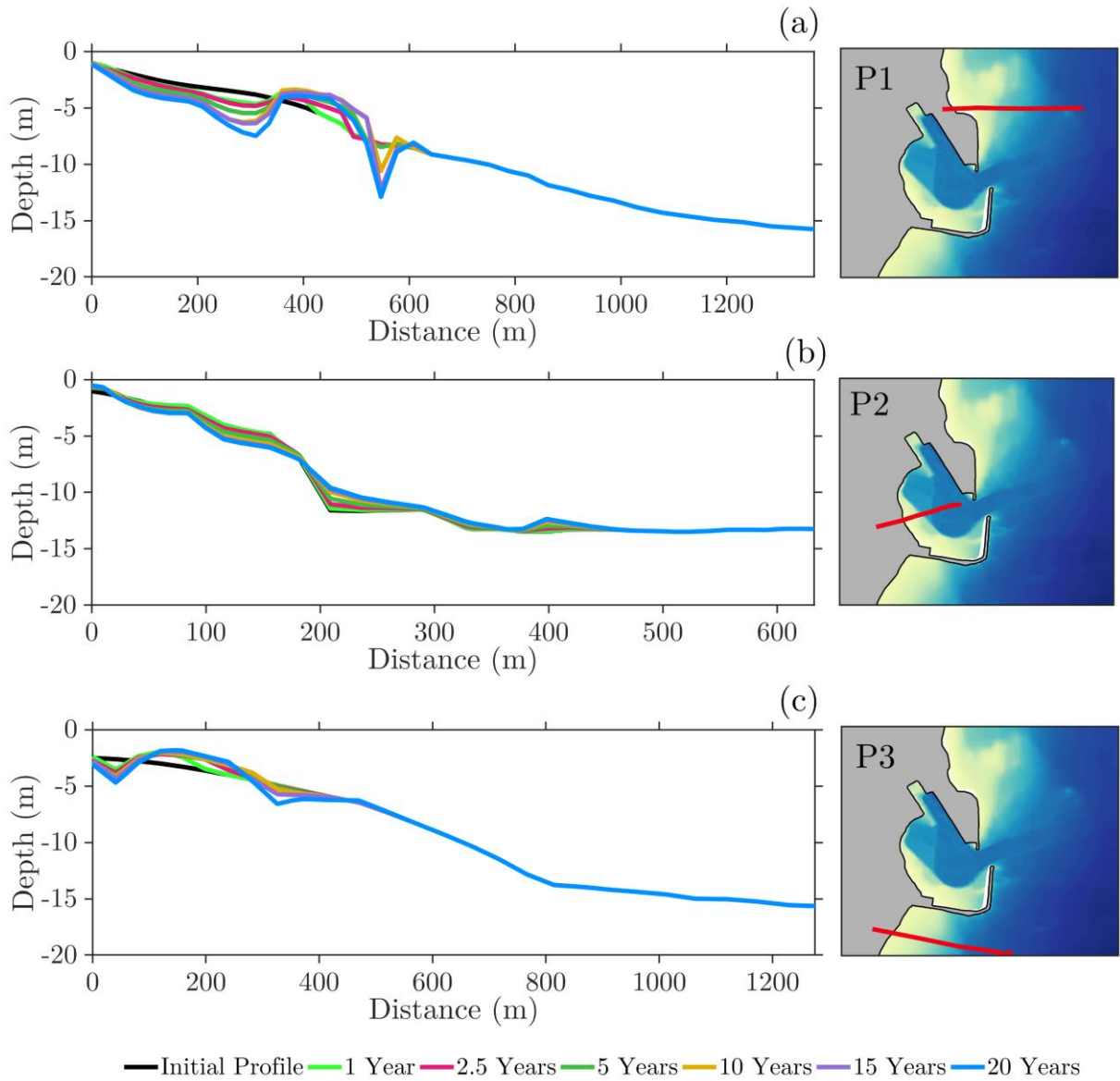
which can be intensified by cold fronts and SW winds as observed by Albino *et. al.* (2006). These factors associated with chaotic distribution of abrasion terraces, the narrow beach ridges, the precarious state of conservation of front dunes presents in dissipative beaches intensify the erosion vulnerability of the coast, main characteristic of this coast (ALBINO, 1999; ALBINO, *et. al.*, 2006).

The Figure 5-11 shows the profiles of the morphological evolution for 1, 2.5, 5, 10, 15 and 20 years in comparison with the initial profile. In Figure 5-11.a is observed the profile P1 located north of the port of Portocel.

In this profile is noted the erosion over the years in distance 300 m and an adjacent accretion in 400 m, followed for abrupt erosion area near 600 m of distance. From 600 m of distance all the profiles are superimposed and no difference is observed. The profile P2 (Figure 5-11.b) is located inside of the port of Portocel and it is shown in the begging a slightly erosion until 180 m of distance approximately, followed for accretion area in 200 m and in 400 m. From 400 m the profiles are superimposed and also it is not observed difference. The Figure 5-11.c presented the profile P3 which is located in the south of port of Portocel is registred an erosion area in comparison with initial profile followed of accretion zone and a slight erosion in 300 m of distance and slight accretion adjacent. From 400 m the profiles are superimposed like seen early. As shown the in Figure 5-11 there is an erosion tendency of the coast in all profiles in the end of 20 years.

These results show the erosion of the profile near to the coast and the seaward bar migration. Inside the port sediment from the coast tend to migrate to the navigation channel and bay.

Figure 5-11 – Morphological profiles P1 (a), P2 (b) and P3 (c) located in north, south and inside the port of Portocel for initial profile (black line), 1 year (green line), 2.5 years (magenta line), 5 years (dark green line), 10 years (mustard line), 15 years (purple line) and 20 years (blue line).



Source: Author.

6 CONCLUSIONS AND RECOMMENDATIONS

6.1 CONCLUSIONS

The hydrodynamic, waves, sediment transport and morphological evolution in port of Portocel and surroundings were studied in this work. The results of numerical model were satisfactory when compared with *in situ* measured currents, waves and morphological changes.

The hydrodynamics induced by tide, wind and waves reached the highest depth (~15m), in the proximities of the port of Portocel with high velocities (0.25 m/s), while without the effects of waves and wind the velocities reached low magnitudes (0.05 m/s). The highest velocities found are related to longshore currents generated by waves and wind in north and south of port.

The wave climatology in study area shows the predominance of ESE and E direction, while the maximum magnitude of 1.5 m is found inside the port. Outside of the port, in north and south regions the significant wave heights reached 2.75 m. The waves approaching the coast suffer refraction due to bathymetry and this way they line up in E-W direction. The port's groyne dissipates most of the wave energy and prevent the propagation of the high waves into the port.

The sediment transport is determined mainly by the wave breaking and wind, which intensifies the superficial currents. The bedload sediment transport reached $8 \times 10^{-6} \text{ m}^3/\text{s}/\text{m}$ while the suspended sediment transport reached $4.5 \times 10^{-5} \text{ m}^3/\text{s}/\text{m}$.

The different Morfac approaches used in this work shown that there is no significant difference between Morfac tests (1, 30, 60, 90). Therefore, the Morfac = 90 was utilized for simulation to 20 years. The morphological evolution for 20 years shown that waves and wind were responsible for resuspended and transport of the sediments whose formed the erosion and deposition regions in port of Portocel and surroundings.

The results indicate that in 20 years the main characteristic is the erosion regions adjacent of coast in north and south of port. This kind of information may help projects of coastal management to establish the main areas most prone to occur erosion or deposition, which can improve the coastal management of coastal erosion and deposition by forecasting the seabed changes.

6.2 RECOMMENDATIONS

The erosion and deposition areas are function of the bathymetry. Therefore, it's necessary to update bathymetry for the whole study area which may improve the accuracy of the simulation.

To better represent the morphological evolution changes, it's important to obtain the sediment discharge, flow and sediment bed composition of rivers near the study site (*e.g Rio Riacho*), for a minimum period of 1 year to set reliable estimates riverine sediment contribution.

It's important to elaborate a sample mesh with many points as possible to collect sediment data (grain size) to obtain a most real characterization of sediment distribution in study region and also to discuss the main sediment fractions transported.

In this work a depth-averaged model was set to the port of Portocel. To improve the model results there is a need to simulate 3D flow, including stratification. Simulation of local wind also may lead to a better understanding of wind effects, mainly by sea and land breeze and set the proper wind velocities and directions.

7 REFERENCES

- Abanades, J., Greaves, D., Iglesias, G., Coastal defence using wave farms: the role of farm-to-coast distance. **Renew. Energy**. 75, 572 e 582. 2014.
- Alari, V.; Raudsepp, U.; Kõuts, T. Wind wave measurements and modelling in Küdema Bay, Estonian Archipelago Sea. **Journal of Marine Systems**, v. 74, p. S30-S40, 2008.
- Albino, J. **Processos de Sedimentação atual e morfodinâmica das praias de Bicanga a Povoação, ES**. Tese de doutoramento em Ciências – Instituto de Geociências, Universidade de São Paulo, São Paulo, 1999.
- Albino, J.; Girardi, G.; Nascimento, K. A. **Espírito Santo – Erosão e Progradação do Litoral Brasileiro**. 2006.
- Alves, J.; Ribeiro, E.; Matheson, G.; Lima, J.; Ribeiro, C. Reconstituição do clima de ondas no sul-sudeste brasileiro entre 1997 e 2005. **Revista Brasileira de Geofísica**, v. 27, n. 3, p. 427-445, 2009.
- Ariathurai, C. R. 1974. **A finite element model for sediment transport in estuaries**. Ph.D. Thesis, University of California, Davis.
- Cao, Z., Pender, G. Wallis, S. Carling P. Computational Dam-break hydraulics over erodible sediment bed. **Journal Hydraulic Engineering**. 130. 689-703. 2004.
- Cayocca, F., 2001. Long-term morphological modeling of a tidal inlet: the Arcachon Basin, France. **Coast. Eng.** 42 (2), 115–142 (February).
- Coeffe, Y., Pechon, P. H. Modelling of Sea-Bed evolution under waves action. **Coastal Engineering**. Part II: Coastal Sediment Problems. p. 1149-1160. 1982.
- Coutinho, T. **Alterações Morfológicas do leito no estuário formado pelos rios Piraquê-Açú e Piraquê-Mirim**. Trabalho de Conclusão de Curso. Universidade federal do Espírito Santo. Vitória. 2015.
- Curbani, F. **Caracterização de ondas na região adjacente ao porto de Barra do Riacho, Aracruz-ES, para o ano de 2008**. Monografia. Universidade Federal do Espírito do Santo. Vitória. 2011.
- Dastgheib, A., Roelvink, J.A., Wang, Z.B., Long-term process-based morphological modeling of the Marsdiep Tidal Basin. **Mar. Geol.** 256, 90e100. 2008.
- DELTAES. **Delft3D Flow User Manual**. Delft. 2011.
- DELTAES. **Delft3D Wave User Manual**. Delft. 2014.
- Ding, Y., Wang, S. S. Y. Development and validation of a quasi-three-dimensional coastal area morphological model. **Journal of waterway, port, coastal, and ocean engineering**. 132. 462-476. 2006.

Dissanayake, D.M.P.K., Ranasinghe, R., Roelvink, J.A., The morphological response of large tidal inlet/basin systems to Relative Sea level rise. **Climatic Change**, <http://dx.doi.org/10.1007/s10584-012-0402-z>. 2012.

Dissanayake, D.M.P.K., Roelvink, J.A., Van der Wegen, M. Modelled channel pattern in schematised tidal inlet. **Coastal Engineering** 56, 1069–1083. 2009.

Dongeren, A. R., Vriend, H. J. A model of morphological behavior of tidal basins. **Coastal Engineering**. 22. 287-310. 1994.

Dunn, R.; Zigic, S.; Burling, M.; Lin, H. Hydrodynamic and Sediment Modelling within a Macro Tidal Estuary: Port Curtis Estuary, Australia. **Journal of Marine Science and Engineering**. v. 3, n. 3, p. 720-744, 2015.

Dwarakish, G. S., Salim, A. Review on the Role of Ports in the Development of a Nation. *Aquatic Procedia*, v. 4, p. 295-301, 2015.

ECMWF – European Center for Medium-Range Weather Forecasts. Available in : <<https://confluence.ecmwf.int/display/FUG/2.1+Global+Atmospheric+Model>>. Access in: 20 april 2019.

Egbert, G.D., Erofeeva, S.Y. Efficient Inverse Modeling of Barotropic Ocean Tides. *Journal of Atmospheric and Ocean Technology*. v. 19, p. 183–204. 2002.

Engelund, F., Hansen, F. **A Monograph of Sediment Transport in Alluvial Channels**. Teknisk Forlag, Copenhagen. 1967.

Exner, F. M. Über die Wechselwirkung zwischen Wasser und Geschiebe in Flüssen. *Akad. Wiss. Wein Math. Naturwiss. Klasse*. 134(2a). p. 929-952. 1925.

FEMAR. **Catalogo de estações maregráficas brasileiras (Catalog of Brazilian tidal stations)**. Compiled by F.J.P. Salles, F.C.M. Bentes and J.A. Santos — Fundação de Estudos do Mar (Ocean Studies Foundation), Rio de Janeiro, Brazil, 280pp. 2000.

García Alba, J.; Gómez, A.; Tinoco López, R. et al. A 3-D model to analyze environmental effects of dredging operations – application to the Port of Marin, Spain. **Advances in Geosciences**. v. 39, p. 95-99, 2014.

Gelfenbaum, G., Roelvink, J. A., Meijs, M. Buijsman, M. Ruggiero, P. Process-based morphological modeling of Gray Harbor inlet at decadal timescales. **Proceedings of Coastal Sediments'03**. 2003.

Gerritsen, H., Goede, E.D., Platzek, F.W., Genseberger, M., Kester, J.A., Uittenbogaard, R. E. **Validation Document Delft3d-Flow -A Software System for 3D Flow Simulations**. WL | Delft Hydraulics, 2007.

Gorman, R.; Bryan, K.; Laing, A. Wave hindcast for the New Zealand region: Nearshore validation and coastal wave climate. **New Zealand Journal of Marine and Freshwater Research**, v. 37, n. 3, p. 567-588, 2003.

Gu, Z., Zhang, C., Zheng, J. Influences of wave forcing and morphological variability on the evolution of a double-sandbar system. **Journal of engineering for the maritime environment**. 230 (3). 467-480. 2016.

Guillas, S, Bakare, A., Morley, J. et al. Functional autogressive forecasting of long-term seabed evolution. *J Coastal Conservation*. 15:337-351. 2011.

Guo Q., Jin, Y. Modeling sediment transport using depth-averaged and moment equations. **J. Hydraul. Eng.** 125. 1262-1269. 1999.

JIA, L.; WEN, Y.; PAN, S.; LIU, J. T.; HE, J. **Wave-current nteraction in a river and wave dominant estuary: A seasonal contrast**. *Applied Ocean Research*. v. 52. p. 151-166. 2015.

Kim, J., Park, J., 2015. Ocean & coastal management mathematical modeling of coastal marine environments using observational data for coastal management. *Ocean Coast. Manag.* 116, 396e403.

Kleinhans, M. G.; Grasmeijer, B. T. Bed load transport on the shoreface by currents and waves. **Coastal Engineering**. v. 53. p. 983-996. 2006.

Komen, G.; Hasselmann, K.; Hasselmann, K. On the Existence of a Fully Developed Wind-Sea Spectrum. **Journal of Physical Oceanography**, v. 14, n. 8, p. 1271-1285, 1984.

Kuang, C., Liu, X., Jie et al. Numerical prediction of medium-term tidal flat evolution in the Yangtze Estuary: Impacts of the Three Gorges project. *Continental Shelf Research*, v. 52, p. 12-26, 2013.

LABORATÓRIO DE TRANSPORTES E LOGÍSTICA – LABTRANS. **Plano mestre – barra do Riacho**. Florianópolis, SC. 2015.

Lee, B.; Chien, H.; Cheng, H.; Chiou, M. Evaluation of Operational Wave Forecasts for the Northeastern Coast of Taiwan. **Terrestrial, Atmospheric and Oceanic Sciences**, v. 21, n. 1, p. 195, 2010.

Lesser, G. R. **An approach to Medium-term Coastal Morphological Modelling**. Thesis of Doctor degree. Delft University of Technology. Delft, The Netherlands. 2009.

Lesser, G. R.; Roelvink, J. A.; Kester, J. A. T. M.; Stelling, G. S. Development and validation of a three-dimensional morphological model. **Coastal Engineering**. v. 51. p. 883-915. 2004.

LI, L. **A Fundamental study of the morphological acceleration fator**. Master thesis. Deltares. P. 120. 2010.

- Lu, Q., Nairn, R. B. Prediction on morphological response of dredge sand-borrow pits. **Coastal Engineering**. 2010.
- Mayerle, R.; Narayanan, R.; Etri, T.; Abd Wahab, A. A case study of sediment transport in the Paranagua Estuary Complex in Brazil. **Ocean Engineering**, v. 106, p. 161-174, 2015.
- Nogueira, I. C. M. **Caracterização sazonal de ondas na região adjacente ao porto de Ubu, Anchieta – ES, para o ano de 2008**. Monografia. Universidade Federal do Espírito Santo. 2010.
- Padilla-Hernández, R.; Perrie, W.; Toulany, B.; Smith, P. Modeling of Two Northwest Atlantic Storms with Third-Generation Wave Models. **Weather and Forecasting**, v. 22, n. 6, p. 1229-1242, 2007.
- Partheniades, E. 1965. Erosion and deposition of cohesive soils. **Journal of the Hydraulics Division Proceedings of the ASCE**. v. 9. p. 105–139.
- Piumbini, P. P. **Clima de ondas de gravidade e estado de agitação marítima em ambientes marinhos no Espírito Santo**. Dissertação de mestrado. Centro Tecnológico, Departamento de Engenharia Ambiental, Universidade Federal do Espírito Santo, Vitória, ES, Brasil. 2009.
- PORTOCEL (Terminal Especializado de Barra do Riacho). Navegação e Manobra. Disponível em: < <http://www.portocel.com.br/pt/navegacao.htm>>. Acesso em: 05 fev. 2017.
- Ports of Australia. Dredging and Australian Ports: Subtropical and Tropical Ports. Sprott – planning & environment. 2014.
- Prumm M., Iglesias G. Impacts of port development on estuarine morphodynamics: Ribadeo (Spain). **Ocean & Coastal Management**. 130. 58-72. 2016.
- Rakha K. A., Deigaard R., Brøker, I. A phase-resolving cross shore sediment transport model for beach profile evolution. **Coastal Engineering**. 31. 231-261. 1997.
- Rijn, L. C. van. Unified view of sediment transport by currents and waves. I: Initiation of motion, bed stress and bed load transport. **Journal of Hydraulic Engineering**. 133(6): 649-667. 2007.
- RIJN, L. C. van; WALSTRA, D. J. R. 2003. **Modelling of sand transport in Delft3D**. Delft Hydraulics. [S.l.].
- Rogers, W.; Hwang, P.; Wang, D. Investigation of Wave Growth and Decay in the SWAN Model: Three Regional-Scale Applications. **Journal of Physical Oceanography**, v. 33, n. 2, p. 366-389, 2003.

Rosenhagen, A. G. J.; **Aplicação de uma fórmula de transporte de sedimentos considerando ondas e correntes em um modelo hidro-sedimentológico**. Dissertação de Mestrado. Instituto Alberto Luiz Coimbra de Pós-Graduação e Pesquisa de Engenharia. COPPE – Universidade Federal do Rio de Janeiro. Rio de Janeiro. 2013.

Ruggiero, P., Buijsman, M., Kaminsky, G. M., Gelfenbaum, G. Modeling the effects of wave climate and sediment supply variability on large-scale shoreline change. **Marine geology**. 273. 127-140. 2010.

Ruggiero, P., Walstra, D.J.R. Gelfenbaum, G. et al. Seasonal-scale nearshore morphological evolution: Field observations and numerical modeling. **Coastal Engineering**, v.56, n. 11-12, p. 1153-1172, 2009.

Rusu, E.; Pilar, P.; Guedes Soares, C. Evaluation of the wave conditions in Madeira Archipelago with spectral models. **Ocean Engineering**, v. 35, n. 13, p. 1357-1371, 2008b.

Rusu, L.; Pilar, P.; Guedes Soares, C. Hindcast of the wave conditions along the west Iberian coast. **Coastal Engineering**, v. 55, n. 11, p. 906-919, 2008a.

Rusu, L.; Pilar, P.; Bernardino, M; Guedes Soares, C. Hindcast studies of the wave conditions on the Portuguese coast. **Marine Technology and Engineering**. p. 181-198. 2011.

Shu-Hua, Z., Ning-Chuan, Z., Bei, L., Zheng, Z., Zhi-Xia, Z. Numerical simulation of tidal current and erosion and sedimentation in the Yangshan deep-water harbor of Shanghai. **International journal of sediment research**. 24. 287-298. 2009.

Silva, A. E.; Quaresma, V. S.; Bastos, A. C. Sedimentological sectorization of an estuarine in a regressive coast, southeast Brazil. **Journal of Sedimentary research**. v. 83. p. 994-1003. 2013.

Sivakholundu K. M., Vijaya, R., Kiran, A. S. Abhishek, T. Short term morphological evolution of sandy beach and possible mitigation: A case study off Kadalur Periyakuppam. **Indian Journal of Geo-Marine Sciences**. 43 (7). 1297-1305. 2014.

SMS - Brasil - Sistema de Modelagem Costeira. Available in: <<http://smcbrasil.ihcantabria.com/ihdata-onda/>>. Access in: 20 april 2019.

Spearman, J.R., Dearnaley, M.P.Dennis, J.M. A simulation of estuary response to training wall construction using a regime approach. **Coastal Engineering**, v. 33, n. 2-3, p. 71-89, 1998.

Thatcher, M. L., And D. R. F. Harleman. **A mathematical model for the prediction of unsteady salinity intrusion in estuaries**. Tech. Rep. 144, Department of Civil Engineering, Massachusetts Institute of Technology Cambridge. 1972.

THE SWAN TEAM. **SWAN – Scientific and Technical Documentation**. Delft University of Technology. p. 140. 2016.

van der Wegen, M., **Modeling Morphodynamic Evolution in Alluvial Estuaries** (Ph.D thesis). Delft University of Technology. 2010.

Van der Wegen, M., Roelvink, J.A., De Ronde, J., Van der Speck, A., Long-term morphodynamics evolution of the Western Scheldt estuary, The Netherlands, using a process-based model. COPEDEC VII, Dubai, UAE. 2008.

Van Maren, D. S., van Kessel, T., Cronin, K., Sittoni, L. The impact of channel deepening and dredging on estuarine sediment concentration. **Continental Shelf Research**. 95. 1-14. 2015.

van Rijn, L.C., 2007. Unified view of sediment transport by currents and waves. I: initiation of motion, bed roughness, and bed-load transport. *J. Hydraul. Eng.* 133, 649e667.

Verboom, G. K.; Slob, A. Weakly-reflective boundary conditions for two-dimensional shallow water flow problems. **Advance Water Resources**. v. 7. 1693-1708. 1984.

Vested, H. J., Tessier, C. Cristensen B. B., Goubert, E. Numerical modelling of morphodynamics. **Ocean Dynamics**. 63. 423-446. 2013.

Vijverberg, T.; Reneerkens, M.; Winterwerp, H.; Scholl, O.; Haruna, Y. Sediment dynamics in lagos harbour - reconnaissance on effects of dredging. **Coastal Engineering Proceedings**, v. 1, n. 33, 2012.

Vriend H. J., Zyserman J., Nicholson, J., Roelvink J. A., Péchon, P. and Southgate H. N. Medium-term 2DH coastal area modelling. **Coastal Engineering**. 21. 193-224. 1993.

Wang J., Dong, J., Huang J., Chen Z., Xu, S. Evolution trend analysis of nearshore seabed in Yandshan Deep-water Port, China. *J. Coast Conserv.* 18: 17-25. 2014.

Wang, Q. Kang, H. A three-dimensional modeling of the morphological change in the Liaodong Bay. **Frontiers of Earth Science**. v. 9, n. 3, p. 509-520, 2015.

Wang, Y., Tang, L., Wang, C., Liu, C., Dong, Z. Combined effects of channel dredging, land reclamation and long-range jetties upon the long-term evolution of channel-shoal system in Qinzhou Bar, SW, China. **Ocean Engineering**. 91. 340-349. 2014a.

Wang, Y.; Wang, C.; Tang, L. et al. Long-term morphological response to dredging including cut-across-shoal in a tidal channel-shoal system. **Ocean Dynamics**. v. 64, n. 12, p. 1831-1843, 2014b.

Wang, Z.; Louters, T.; de Vriend, H. Morphodynamic modelling for a tidal inlet in the Wadden Sea. *Marine Geology*, v. 126, n. 1-4, p. 289-300, 1995.

Wei, X., Wu, C. Long-term process-based morphodynamics modeling of the Pearl River Delta. **Ocean Dynamics**. 64. 1753-1765. 2014.

Wijnberg K, Terwindt J. Extracting decadal morphological behavior from high-resolution, long-term bathymetric surveys along the Holland coast using eigenfunction analysis. *Mar Geol.* 126:301-330. 1995.

Wu, Chengqiang, Cai, FengZhao, Guangtao et al. Impact of coastal engineering constructions on the topographic and morphological evolution of Quanzhou Bay, Fujian, China. *Ocean & Coastal Management*, v. 54, n. 7, p. 544-555, 2011.

Xie, D., Gao, S., Wang, Z., Pan, C. Numerical modeling of tidal currents, sediment transport and morphological evolution in Hangzhou Bay, China. **International Journal of Sediment Research**. 28. 316-328. 2013.

Xu, T., You, X. Simulation of morphological changes induced by large-scale coastal engineering using a 3D wave-current interaction model. **Indian Journal of Geo-Marine Science**. 25 (2). 215-223. 2016.

Ying, X.; Ding, P.; Wang, Z.; Van Maren, D. Morphological Impact of the Construction of an Offshore Yangshan Deepwater Harbor in the Port of Shanghai, China. **Journal of Coastal Research**. v. 278, p. 163-173, 2012.